Article

Not peer-reviewed version

A Novel Remote Sensing–Derived Indicator for Monitoring Watershed-Scale Ecological Pressure on Tributary Eutrophication in a Large Reservoir System

Abdelrahman Hassan , Oluwafemi Adewole Adeyeye , Wei Huang , Xiaojiao Luo , Yemei Kong , Bai Guoxin , Zenghui Song , Guanglang Yang , Xuexing Yao , Muhammad Waqas Yonas , Amechi S. Nwankwegu , Yan Zhang , Shuai Wang * , Lei Zhang *

Posted Date: 29 April 2026

doi: 10.20944/preprints202604.2015.v1

Keywords: Net Ecological Pressure Index; landuse/landcover data; spatio-temporal analysis; river eutrophication; integrated water resources management; Three Gorges Reservoir Region

Article

A Novel Remote Sensing–Derived Indicator for Monitoring Watershed-Scale Ecological Pressure on Tributary Eutrophication in a Large Reservoir System

Abdelrahman Hassan [1,2,3], Oluwafemi Adewole Adeyeye [1,2], Wei Huang [1,2], Xiaojiao Luo [1,2], Yemei Kong [1,2], Bai Guoxin [1,2], Zenghui Song [1,2], Guanglang Yang [1,2], Xuexing Yao [1,2], Muhammad Waqas Yonas [1,2], Amechi S. Nwankwegu [1,2], Yan Zhang [1,2,4], Shuai Wang [1,2,*] and Lei Zhang [1,2,*]

[1] College of Resources and Environment, Southwest University, 1 Tiansheng Road, Beibei District, Chongqing 400716, China
[2] International S&T Collaboration Base on Water Environmental Monitoring and Simulation in Three Gorges Reservoir Region, Chongqing 400716, China
[3] Soil and Water Department, Faculty of Agriculture, Suez Canal University, Ismailia 41522, Egypt
[4] Agricultural Bureau, Changshou, Chongqing 401220, China
* Correspondence: shuaiwang@swu.edu.cn (S.W.); echozhanglei@swu.edu.cn or zhanglei@uwindsor.ca (L.Z.)

Highlights

What are the main findings?

- A remote-sensing-derived Net Ecological Pressure Index (NEPI) was developed to quantify watershed-scale ecological pressure on eutrophication based on the balance between agricultural and forest domination.
- NEPI revealed distinct spatial and temporal behavior between northern and southern banks of the Three Gorges Reservoir across backwater sensitivity zones.

What are the implications of the main findings?

- NEPI provides a standardized and transferable indicator for comparing landscape ecological pressure across reservoir tributaries using multi-temporal LULC data.
- The approach supports long-term monitoring and spatial prioritization of eutrophication management in large reservoir systems with mixed agricultural and forest landscapes.

Abstract

Monitoring landscape ecological pressure on river eutrophication requires spatially explicit, temporally comparable indicators derived from remote sensing data. This study develops the Net Ecological Pressure Index ($NEPI_{ws}$) to quantify watershed-scale ecological pressure on eutrophication based on the balance between agricultural and forest domination and ranged from −1 to 1,where positive values reveal domination of agriculture ecological pressure over forests ecological buffering, while negative values reveal the opposite domination pattern. Using 30 m land-use/land-cover data for 2010 and 2024, the spatio-temporal dynamics of $NEPI_{ws}$ was analyzed for 25 1st-order tributaries in the Three Gorges Reservoir Region, including 13 on the northern bank and 12 on the southern bank across reservoir sensitive, sub-sensitive, and non-sensitive zones to account for interaction with backwater effects. Results showed a clear spatial pattern, with $NEPI_{ws}$ increasing on both banks as backwater sensitivity decreased farther from the dam. Cumulative $NEPI_{bank}$ of both banks revealed higher value on the northern bank in the non-sensitive and sub-sensitive zones, while showed higher value on the southern bank in the sensitive zone. From 2010 to 2024, the cumulative $NEPI_{bank}$ exhibited contrasting temporal trends. In the sensitive zone, cumulative $NEPI_{bank}$ increased by 0.0896 on the southern bank, 2.05 times the increase on the northern bank 0.0436. In the sub-sensitive zone, $NEPI_{bank}$ declined more on the northern bank (−0.105) than on the southern bank (−0.0401). In the non-sensitive zone, $NEPI_{bank}$ decreased on the northern bank (−0.0641) but increased on the southern bank (0.0242). Overall, NEPI effectively captured spatio-temporal variations in watershed-scale ecological pressure on tributary eutrophication using Earth observation data. Its standardized and transferable formulation enables comparative assessment, eco-functional zoning and spatial prioritization of eutrophication management in large reservoir systems, demonstrating the value of remote sensing data for integrated water resources management in mixed agricultural–forest landscapes.

Keywords: Net Ecological Pressure Index; landuse/landcover data; spatio-temporal analysis; river eutrophication; integrated water resources management; Three Gorges Reservoir Region

1. Introduction

One of the defining characteristics of the anthropocene is the increasing emergence of complex environmental threats with spatio temporal dimensions [1-3]. Among these threats, river eutrophication has become a serious global concern for water resources security since the 20th century, largely driven by rapid economic development [4]. As surficial sign of eutrophication, harmful algal blooming events (HABs) disrupt aquatic ecosystem functions in numerous rivers and tributaries, diminishing their capacity to provide essential ecosystem services for human well-being [5].

Having 415,000 ha of farmlands in 2017, the Three Gorges Reservoir Region (TGRR) located in the middle of Yangtze River basin represents one of the most ecologically-sensitive hot spots in China due to river eutrophication mainly driven by agricultural non-point source pollution from intensified agriculture activities [6-8]. Furthermore, the impoundment of the Three Gorges Dam (TGD) in 2003 added new dimensions to ecological sensitivity in the region [9]. Due to hydrodynamic effect of the Three Gorges Reservoir (TGR) impoundment, the 1st-order tributaries of TGRR experienced a significant decline in flow velocity which increased water retention and nutrient storage time converting number of these tributaries into bloomed rivers [10,11]. Moreover, the 1st-order tributaries along TGRR receives contrast quantities of nutrient loads with backwater confluence from the main stem of Yangtze River [12,13].

Ecological sensitivity in the TGRR is fundamentally shaped by the interaction of two major sources of ecological pressure: Agricultural Ecological Pressure (AEP), driven by intensive farming activities [14-16], and Backwater Ecological Pressure (BEP), resulting from the hydrodynamic effects of the Three Gorges Reservoir [10,17-19]. However, ecological sensitivity is not determined by pressure alone; rather, it arises from the balance between ecological pressure and ecosystem buffering capacity [20-22]. In this context, forest land cover serves as an important ecological buffer, functioning as an effective sink for sediments and nutrients and thereby helping to mitigate eutrophication risk [23,24].

Most existing studies have emphasized reservoir-induced hydrodynamic effects as a primary driver of algal bloom formation in the 1st -order tributaries of the TGRR [25,26]. However, this explanation alone appears insufficient, given that only 50% of these tributaries (20 out of 40) have experienced frequent algal blooms, whereas the remaining 20 tributaries have rarely reported bloom events since 2003 [27]. Recently, Xu et al. [19] simulated the hydrodynamic sensitivity of the 1st-order tributaries to water table changes in the TGR during the flooding, drawdown, and impoundment stages. During the impoundment stage, the northern-bank and southern-bank the 1st -order tributaries were combined into three distinct backwater sensitivity zones with respect to distance from TGD i.e., sensitive zone, sub-sensitive zone and non-sensitive zone implying that tributaries within each zone are exposing to similar hydrodynamic effect. Despite being subjected to the same hydrodynamic effect during the TGR impoundment stage, the northern-bank tributaries revealed higher eutrophication levels compared to the southern-bank tributaries (Figure S1) as shown by a survey study for water quality variation in the 1st-order tributaries of TGRR from 2000 to 2015 [10,19]. These evidences suggested a contrasting spatial ecological sensitivity among 1st-order tributaries of the TGRR, which couldn't be comprehensively explained based on hydrodynamic influence of the TGR alone which usually estimated as a function to distance from TGD [19]. They further demonstrated that a differentiated ecological function for tributary locality on one of TGRR banks is expected to shape the eutrophic susceptibility of 1st-order tributaries on both banks under similar hydrodynamic conditions. In this context, the integration between sources of ecological pressures controlling eutrophication evolution can provide strong alternative approach for integrated water resources management. This arises the need for eco-functional zoning to identify the unique combinations of eutrophication drivers along the TGRR northern and southern banks and enable informed management decisions and evaluate eutrophication mitigation priorities in the TGRR [28,29].

From a different perspective, the association between watershed-scale land-use/land-cover (LULC) composition and surface water quality is well established and supported by several empirical and physical-based modelling studies [30–37]. At watershed scale, researchers reported the strong association of agricultural domination to eutrophication in the 1st - order tributaries of the TGRR [38,39], while others highlighted the positive influence of forest domination on the ecological water quality of the TGR's tributaries [40]. In this context, the interactions between agriculture landuse and forest landcover at watershed scale, have been known as a critical driver of aquatic ecosystem resilience [32,41,42].

Leveraging the unprecedented availability of global data record, remote sensing technologies have demonstrated remarkable potential for assessing environmental vulnerability across space and time [3, 43-45]. Additionally, emerging remote sensing initiatives provide wide range of LULC datasets with multi-spatial and temporal resolutions derived from spectral indices and machine learning approaches for Earth observation applications [46-54]. Also, it supports the ability of environmental planners and ecological decision makers to directly interpret and understand the vulnerability of different ecosystems to various ecological pressures induced by anthropogenic activities i.e., agriculture, mining industrial, urban expansion activities. This study aimed to develop a remote sensing-driven eco-functional zoning framework that integrate sources of ecological pressure, i.e., landscape ecological pressure and backwater ecological pressure to identify the unique combinations of eutrophication drivers along the TGRR northern and southern banks and enable informed management decisions and evaluate eutrophication mitigation priorities in the TGRR. Empowered by the ultimate spatio-temporal capabilities of remote sensing technology, the proposed framework relied on a novel indicator for monitoring landscape ecological pressure on river eutrophication namely the Net Ecological Pressure Index (NEPI), based on watershed-scale agriculture and forests domination ratios. The proposed indicator can be derived based on open-source LULC datasets produced based on optical remote sensing data and capable to capture ecological pressure induced by agriculture activities expansion and analyses its drivers at multi-spatial and temporal scales. The proposed indicator can be incorporated in various ecological implications to provide remote-sensing driven aid and can pave the bridge between mapping ecological hazard and ecological vulnerability.

To achieve the objectives of this study, the following tasks will be fulfilled:

1. Validating the capability of the proposed NEPI to capture the watershed-scale spatio-temporal variability of landscape ecological pressure;
2. Evaluating the feasibility of the proposed NEPI to differentiate the distinct landscape ecological behavior characterizing each of TGRR northern and southern banks across different backwater sensitivity zones on a spatio-temporal basis;
3. Identifying the Unique Eco-Functional Zones (EFZs) across the TGRR;
4. Evaluation of NEPI interoperability at various spatial and temporal scales and highlighting feasibility for remote sensing-driven ecological implications and
5. Revealing NEPI methodological limitations, further investigation needed and potential of future developments.

 doi:10.20944/preprints202604.2015.v1

We believe that valuable lessons can be extracted from this study that can be applicable in large reservoir regions worldwide, certainly where mixed agriculture and forest domination patterns govern the landscape ecological pressure behavior.

2. Materials and Methods

2.1. The Three Gorges Reservoir Region

The Three Gorges Reservoir Region (TGRR) is a highly regulated river–reservoir system located along the middle–upper reaches of the Yangtze River in central China, extending approximately 660 km from Yichang City to Chongqing Municipality and covering about 58,000 km^2 (Figure 1). Following the construction and operation of the Three Gorges Dam, which reached its normal impoundment level of 175 m in 2010, the TGRR has undergone substantial alterations in hydrological and hydraulic processes, including reduced flow velocity, prolonged water residence time, and pronounced seasonal water level fluctuations, particularly within tributary backwater zones [9,17,19]. The region is characterized by complex mountainous terrain with steep slopes and a subtropical monsoon climate, where 70% of annual precipitation occurs during the flood season, intensifying soil erosion risks and non point source pollution transport [10,12,61]. Agricultural non point source pollution from sloping croplands represents a dominant nutrient input, while spatially heterogeneous forest cover plays a critical role in moderating runoff and nutrient export [7,8,23,42]. As a result of the coupled effects of reservoir regulation and landuse change, seasonal algal blooms have been widely reported in 1st-order tributaries, posing significant threats to water quality and ecological security [5,6,11,18]. Owing to these complex land–hydrology–ecosystem interactions under intensified human influence, the TGRR is widely regarded as a representative case for studying landscape ecological pressure in large reservoir systems under anthropocene conditions [1,2].

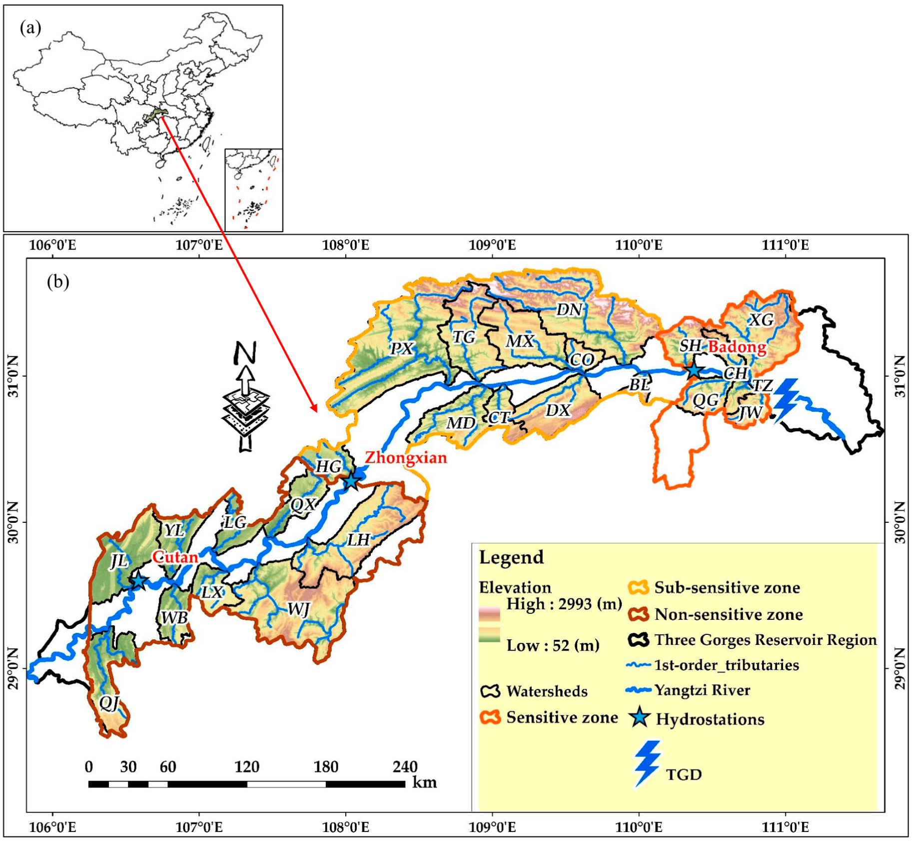

Figure 1. Location of the study area (a) China, (b) selected northern and southern-bank 1st -order tributaries of the Three Gorges Reservoir Region. Northern-bank tributaries included : XG: Xiangxi, CH: Chuxi, SH: Shennong,

Preprints.org (www.preprints.org) | NOT PEER-REVIEWED | Posted: 29 April 2026 doi:10.20944/preprints202604.2015.v1

DN: Daning, CO: Caotang, MX: Meixi, TG: Tangxi, PX: Pengxi,HG:Huangjin,QX:Quxi,LG:Longxi,YL:Yulin,JL:Jialing.Southern-bank tributaries included: JW: Jiuwan, TZ: Tongzhuang, QG: Qinggan, BL: Baolong, DX: Daxi, CT: Chantang, MD: Modao, LH: Longhe, WJ: Wujiang, LX: Lixiang ,WB: Wubu ,QJ: Qijiang.

2.2. Dual-Source Integrated Framework for Eco-Functional Zoning in the TGRR

This study developed a novel remote sensing-driven dual-source integrated framework to interpret the contrasting ecological vulnerability to eutrophication risk among 1st-order tributaries subjected to similar hydrodynamic effects based on identifying the unique combinations of eutrophication drivers along the TGRR northern and southern banks. The framework was established on the existence of two main sources of ecological vulnerability governing eutrophication evolution in the 1st-order tributaries of TGRR: (i) Backwater-Induced Ecological Vulnerability (BIEV), as response to Backwater Ecological Pressure (BEP) driven by reservoir operation regulations, (ii) Landscape-Induced Ecological Vulnerability (LIEV), as response to the Net Landscape Ecological Pressure (NLEP) imposed by watershed-scale LULC domination patterns certainly agriculture and forests domination patterns as key LULC elements across TGRR watersheds [40].

2.2.1. Delineation of TGR Backwater Sensitivity Zones Encompassing Northern and Southern Bank 1st-Order Tributaries

Based on the two-dimensional hydrodynamic modeling, Xu et al. [19] identified the spatial boundaries of TGR backwater sensitivity zones encompassing northern and southern bank 1st -order tributaries during the impoundment stage. Main three sensitivity zones were identified (Figure 1): (i) the sensitive zone, extending from Baodong hydrostation to the TGD affecting tributaries along 76 km of main Yangtze River; (ii) the sub-sensitive zone, extending from Zhongxian to Badong hydrostations and affecting tributaries along 288 km of main Yangtze River; (iii) the non-sensitive zone, extending from Cuntan to Zhongxian hydrostations and affecting tributaries along 240 km of main Yangtze River. To investigate the interaction between both ecological pressure drivers, the spatial domains of main ecologically-sensitive zones encompassing northern and southern bank 1st -order tributaries during the impoundment stage were delineated based on watershed boundaries of the marginal northern and southern tributaries within each zone (Figure 1).

2.2.2. Development of Watershed-Scale Net Ecological Pressure Index (NEPI)

To explore the spatio-temporal dynamics of the Net Landscape Ecological Pressure (NLEP), a novel watershed-scale indicator, the Net Ecological Pressure Index (NEPI $_{ws}$) was developed (Figure 2). The Net Landscape Ecological Pressure (NLEP) can be conceptually defined as the net difference between Agricultural Ecological Pressure (AEP) and Forest Ecological Buffering (FEB) which is mathematically expressed by equation (1):

$$NLEP = AEP - FEB \tag{1}$$

Agriculture Ecological Pressure (AEP) can be conceptually defined as a function of watershed-scale agriculture domination (D_{agrl}) and expressed by equation (2):

$$AEP = f\,(D_{agrl}) \tag{2}$$

Similarly, Forest Ecological Buffering (FEB) can be conceptually defined as a function of watershed-scale forest domination (D_{frst}) and expressed by equation (3):

$$FEB = f\,(D_{frst}) \tag{3}$$

where D_{agrl} and D_{frst} denote watershed-scale agricultural and forests domination, respectively.

To capture spatio-temporal dynamics of the Net Landscape Ecological Pressure (NLEP) at watershed scale based on remote sensing technology, the physical representation for NLEP conceptual components was essential.

At watershed scale, agriculture ecological pressure was physically represented by agriculture domination ratio (AGRL/Watershed ratio) and calculated by equation (4)

doi:10.20944/preprints202604.2015.v1

$$\text{AGRL/Watershed ratio} = A_{agrl,ws}/A_{ws} \tag{4}$$

where $A_{agrl,ws}$ is the agricultural land area (ha) within the watershed and A_{ws} is the total watershed area (ha).

Similarly, at watershed scale, forest ecological buffering was physically represented by forest domination ratio (FRST/Watershed ratio) and calculated by equation (5):

$$\text{FRST/Watershed ratio} = A_{frst,ws}/A_{ws} \tag{5}$$

where A_{frst} is forests area (ha) within the watershed and Aws is the total watershed area (ha).Finally, the proposed watershed-scale Net Ecological Pressure Index ($NEPI_{ws}$) can be physically retrieved by subtracting forest domination ratio from agriculture domination ratio and calculated by equation (6):

$$\begin{aligned} NEPI_{ws} &= \text{AGRL/Watershed ratio} - \text{FRST/Watershed ratio} \\ &= (A_{agrl,ws}/A_{ws}) - (A_{frst,ws}/A_{ws}) \\ &= (A_{agrl,ws} - A_{first,ws})/A_{ws} \end{aligned} \tag{6}$$

$NEPI_{ws}$ values fall within the range -1 and 1, where $NEPI_{ws} > 0$, indicating agricultural domination over watershed landscape and suggesting the domination of agricultural ecological pressure over forest ecological buffering. In addition, $NEPI_{ws} < 0$, indicating forest domination over watershed landscape and suggesting the domination of forest ecological buffering over agricultural ecological pressure.

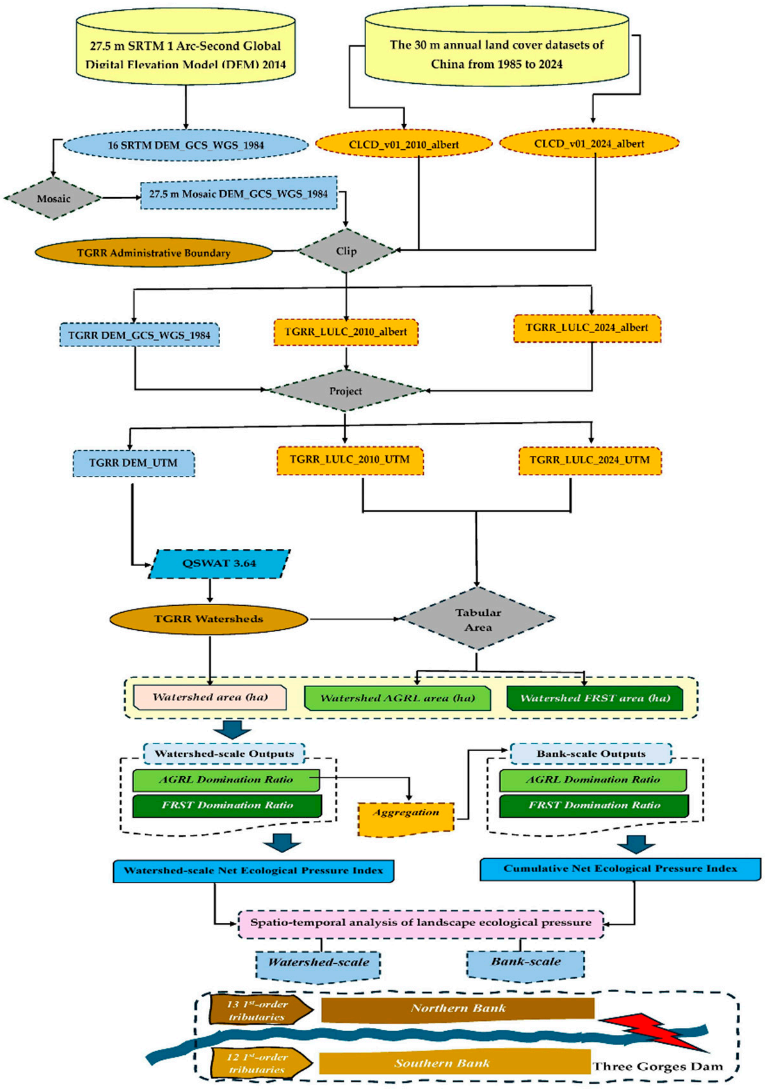

Figure 2. Research framework.

 doi:10.20944/preprints202604.2015.v1

2.2.3. Retrieval of Watershed-Scale LULC Domination Metrics and NEPI

For calculation of agriculture and forest areas a 30 m remote sensing-based landuse/landcover data was downloaded from Zenodo (https://doi.org/10.5281/zenodo.15853565) within two years 2010 and 2024 with accuracy 97 % [46]. For delineation of watershed boundaries and calculation of watershed area 16 SRTM 27.5 m digital elevation model (DEM) downloaded from Earth Explorer (https://earthexplorer.usgs.gov/) . The QSWAT 3_64 (version 1.6) plugin in the QGIS 3.16 software [55] was employed to delineate watershed boundaries based on a 27.5 m digital elevation model (DEM). In this study, to explore the spatio-temporal dynamics of the proposed NEPI $_{ws}$ at watershed scale, 25 TGRR 1st-order tributaries were selected as examples, 13 tributaries located on the northern bank and 12 tributaries located on the southern bank. Using ArcGIS 10.8, the agriculture domination ratio and forest domination ratio were retrieved at watershed scale based on a 30 m landuse/landcover data in 2010 and 2024 [46]. To enable calculation of agriculture and forests areas, the projection system of LULC rasters were converted from Albers system to Universal Transfer Mercator (UTM) system (Figure 2). Using watersheds shapefile delineated from DEM in the previous step, the agriculture and forest areas (m^2) were extracted from LULC rasters for each watershed in 2010 and 2024 (Figures S2 and S3) using Tabulate Area tool in ArcGIS 10.8 (Figure 2).In excel 2016, the agriculture domination ratio and forest domination ratio were calculated respectively from equations (4) and (4), while the Net LULC Ecological Pressure Index (NEPI $_{ws}$) was calculated from equation (6).

2.2.4. Calculation of Cumulative LULC Domination Metrics and Net Ecological Pressure Index (NEPI $_{bank}$)

To identify the cumulative Net Ecological Pressure for each bank within TGR backwater sensitivity zones (NEPI $_{bank}$), the aggregated LULC domination metrics and NEPI $_{bank}$ were calculate from equations (7 and 8):

$$D_{agrl,bank} = \sum A_{agrl,ws} / \sum A_{ws} \quad (7)$$

$$D_{frst,bank} = \sum A_{frst,ws} / \sum A_{ws} \quad (8)$$

where $D_{agrl,bank}$ and $D_{frst,bank}$ represent the cumulative agricultural and forest dominations, respectively, for each bank within TGR backwater sensitivity zones, $\sum A_{agrl,ws}$ and $\sum A_{frst,ws}$ represent the summed agricultural and forest areas (ha) , respectively, and $\sum A_{ws}$ is the total area (ha) for all watersheds on a given bank within TGR backwater sensitivity zones.

Therefore, the cumulative Net Ecological Pressure Index for each bank within TGR backwater sensitivity zones (NEPI $_{bank}$) can be retrieved from equation (9):

$$\begin{aligned} NEPI_{bank} &= D_{agrl,bank} - D_{frst,bank} \\ &= (\sum A_{agrl,ws} / \sum A_{ws}) - (\sum A_{frst,ws} / \sum A_{ws}) \\ &= (\sum A_{agrl,ws} - \sum A_{frst,ws}) / \sum A_{ws} \end{aligned} \quad (9)$$

2.2.5. Identifying the Unique Eco-Functional Zones (EFZs) Across the TGRR

Based on investigation of spatio-temporal dynamics of cumulative NEPI $_{bank}$ for the northern and southern banks across TGR backwater sensitivity zones, the distinct eco-functional zones (EFZs) across TGRR were recognized. To enable multi-scale integrated eutrophication vulnerability assessment across TGRR, a synthesized ranking code was assigned to EFZs at three spatial scales: (i) within the TGR backwater sensitivity zones, (ii) along the northern and southern banks, and (iii) across the entire TGRR system.

3. Results

3.1. Exploring Spatio-Temporal Dynamics LULC Domination and NEPI $_{ws}$ at Watershed Scale

3.1.1. Watershed-Scale Spatial Gradient of LULC Domination and NEPI $_{ws}$ in 2010 and 2024

In 2010 and 2024, both northern and southern-bank 1st -order tributaries of TGRR showed a clear spatial gradient for watershed-scale LULC domination metrics respect to distance to TGD (Figure 3). Interestingly, the watershed-scale agriculture domination and forest domination revealed a reverse spatial gradient across TGR backwater sensitivity zones along both banks (Figure 3). As backwater sensitivity decreased farther from the TGD, watershed-scale agriculture domination showed an increasing trend, while watershed-scale forest domination revealed a decreasing trend along both banks (Figure 3). Correspondingly, the spatial behavior of the watershed-scale Net Ecological Pressure Index (NEPI $_{ws}$) reflected the inverse gradient of the LULC domination metrics (Figure 4). As sensitivity decreased farther from the TGD, NEPI $_{ws}$ values increased along both banks. Moreover, the northern-bank tributaries displayed a stronger spatial gradient in NEPI $_{ws}$ compared with the southern-bank tributaries (Figure 4).

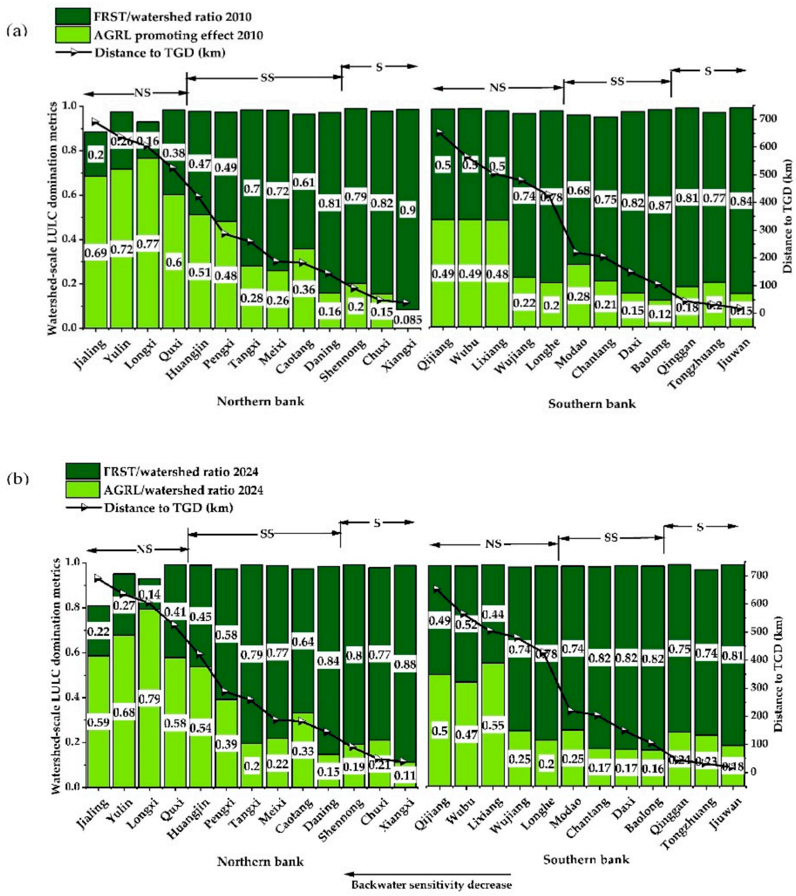

Figure 3. Spatial gradient of LULC domination metrics in 2010 (a) and 2024 (b) of the northern-bank and southern-bank 1st-order tributaries at watershed scale across TGR backwater sensitivity zones regarding distance to TGD and 2024. S refers to' sensitive zone', SS refers to' sub- sensitive zone', NS refers to' non-sensitive zone' according to Xu et al. [19].

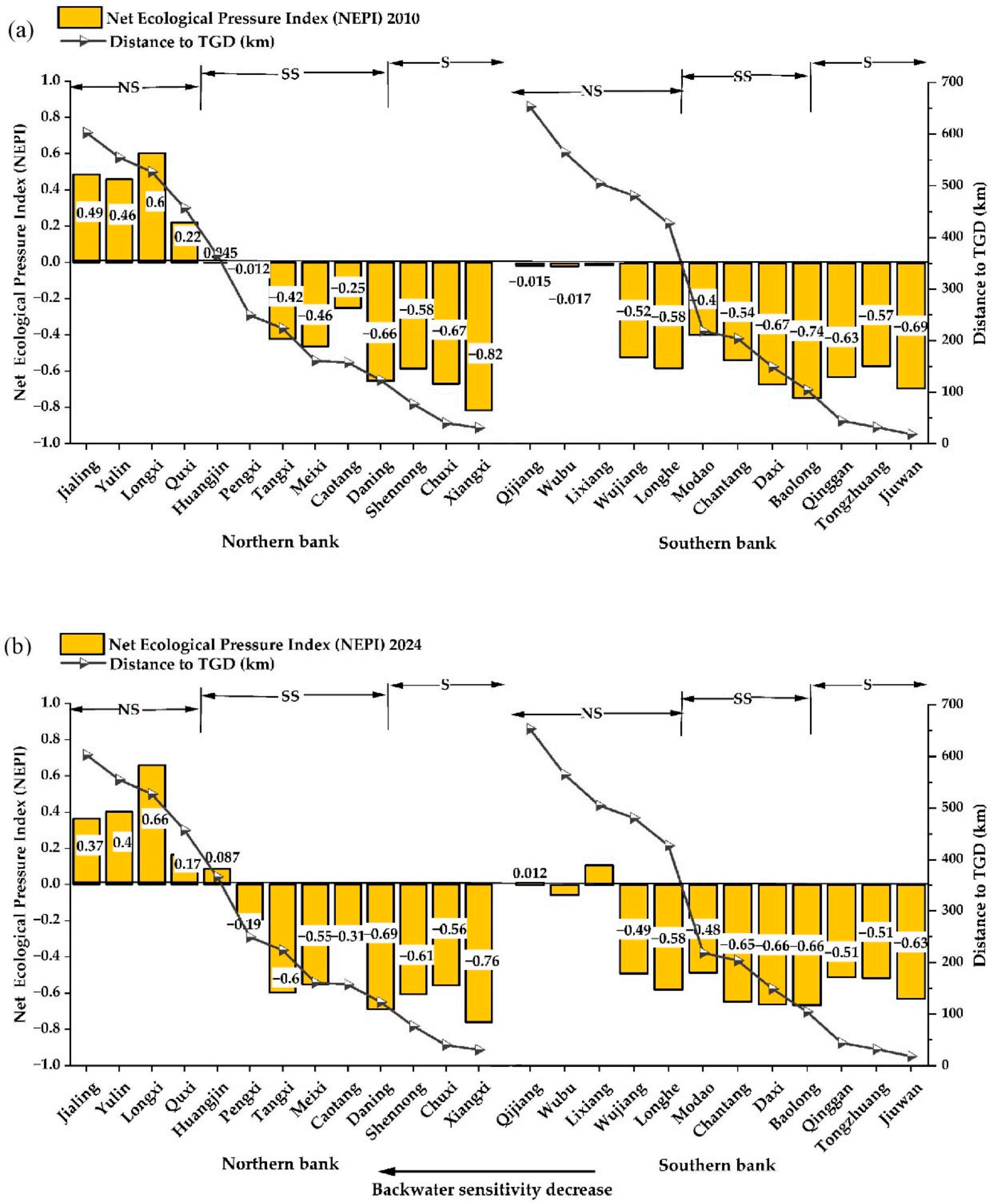

Figure 4. Spatial gradient of NET Ecological Pressure Index (NEPI $_{ws}$) of the northern-bank and southern-bank 1st-order tributaries at watershed scale across TGR backwater sensitivity zones regarding distance to TGD in 2010 (a) and 2024 (b). S refers to' sensitive zone', SS refers to' sub- sensitive zone', NS refers to' non-sensitive zone' according to Xu et al. [19].

3.1.2. Watershed-Scale Temporal Dynamics of LULC Domination and NEPI $_{ws}$ During 2010–2024

Across the TGR backwater sensitivity zones, the temporal changes in watershed-scale LULC domination metrics and NEPI $_{ws}$ exhibited contrasting directions and magnitudes during 2010–2024. Within the sensitive zone, five out of six watersheds showed an increase in agricultural domination and a corresponding decrease in forest domination (Figures 5 and 6a), resulting in increasing NEPI $_{ws}$ values (Figures 5 and 6b). The only exception was the Shennong watershed on the northern bank, which displayed the opposite pattern, with a decrease in NEPI $_{ws}$. Notably, most watersheds with increasing NEPI $_{ws}$ values, i.e., Jiuwan, Tongzhuang, and Qinggan were located on the southern bank (Figure 6).

In contrast, within the sub-sensitive zone, seven out of ten watersheds exhibited a decrease in agricultural domination and an increase in forest domination (Figures 5 and 6a), leading to declining NEPI $_{ws}$ values (Figures 5 and 6b). The remaining three watersheds showed the opposite pattern, with an increase in NEPI. Most watersheds with decreasing NEPI $_{ws}$ values, including Pengxi, Tangxi, Meixi, Caotang, and Danning, were concentrated on the northern bank, showing an increasing spatial gradient for change magnitudes farther from the TGD (Figure 6b). Conversely, two out of three watersheds with increasing NEPI $_{ws}$ values, i.e., Daxi and Baolong, were located on the southern bank (Figure 6b). In contrast, nearly half of watersheds within the non-sensitive zone, four out of nine watersheds, experienced an increase in agricultural domination accompanied by a decline in forest domination (Figures 5 and 6a), which resulted in rising NEPI $_{ws}$ values (Figures 5 and 6b). The remaining four watersheds exhibited the opposite trend, showing increasing forest domination and decreasing agricultural domination, and consequently demonstrated declining NEPI $_{ws}$ values during 2010–2024 (Figures 5 and 6). A unique case was the Longhe watershed, which showed increases in both agricultural and forest domination accompanied by an increase in NEPI $_{ws}$ (Figure 6). Most watersheds with increasing NEPI $_{ws}$, i.e., Longhe, Wujiang, Lixiang, and Qijiang were situated on the southern bank, whereas those with decreasing NEPI $_{ws}$, were predominantly situated on the northern bank, i.e., Quxi, Yulin, and Jialing (Figure 6b).

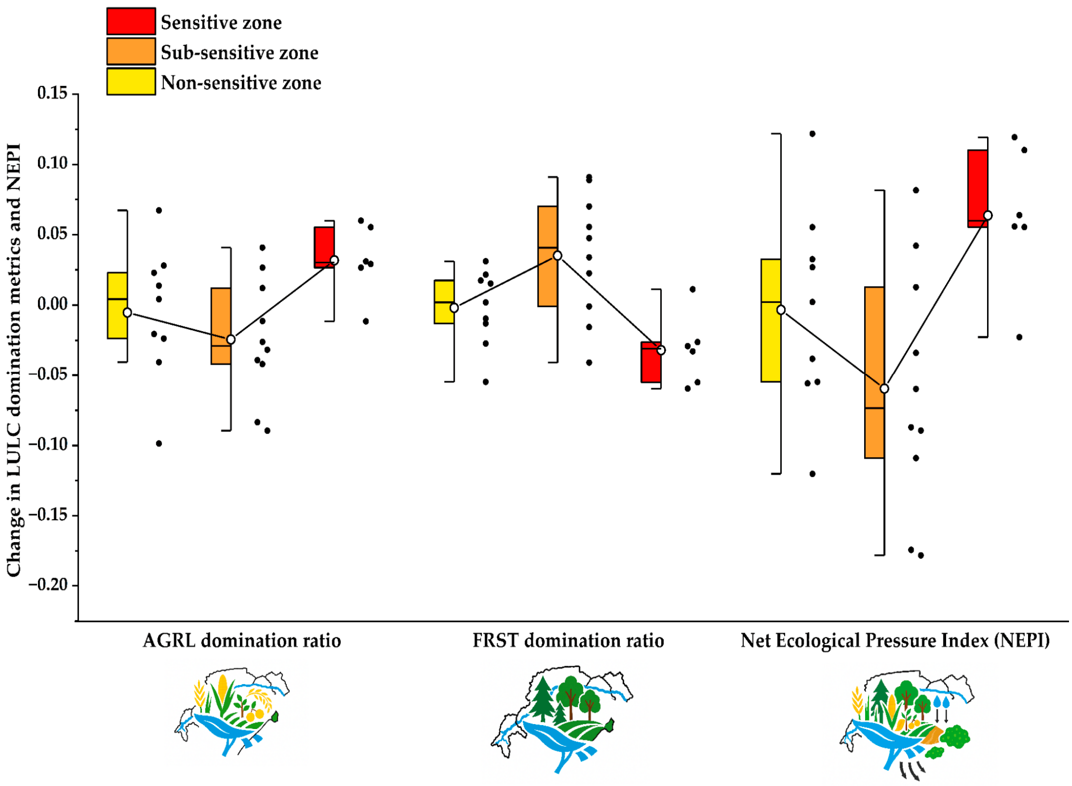

Figure 5. Box plots of the temporal change in the three parameters for watersheds within each sensitivity zone from 2010 to 2024.

Preprints.org (www.preprints.org) | NOT PEER-REVIEWED | Posted: 29 April 2026 doi:10.20944/preprints202604.2015.v1

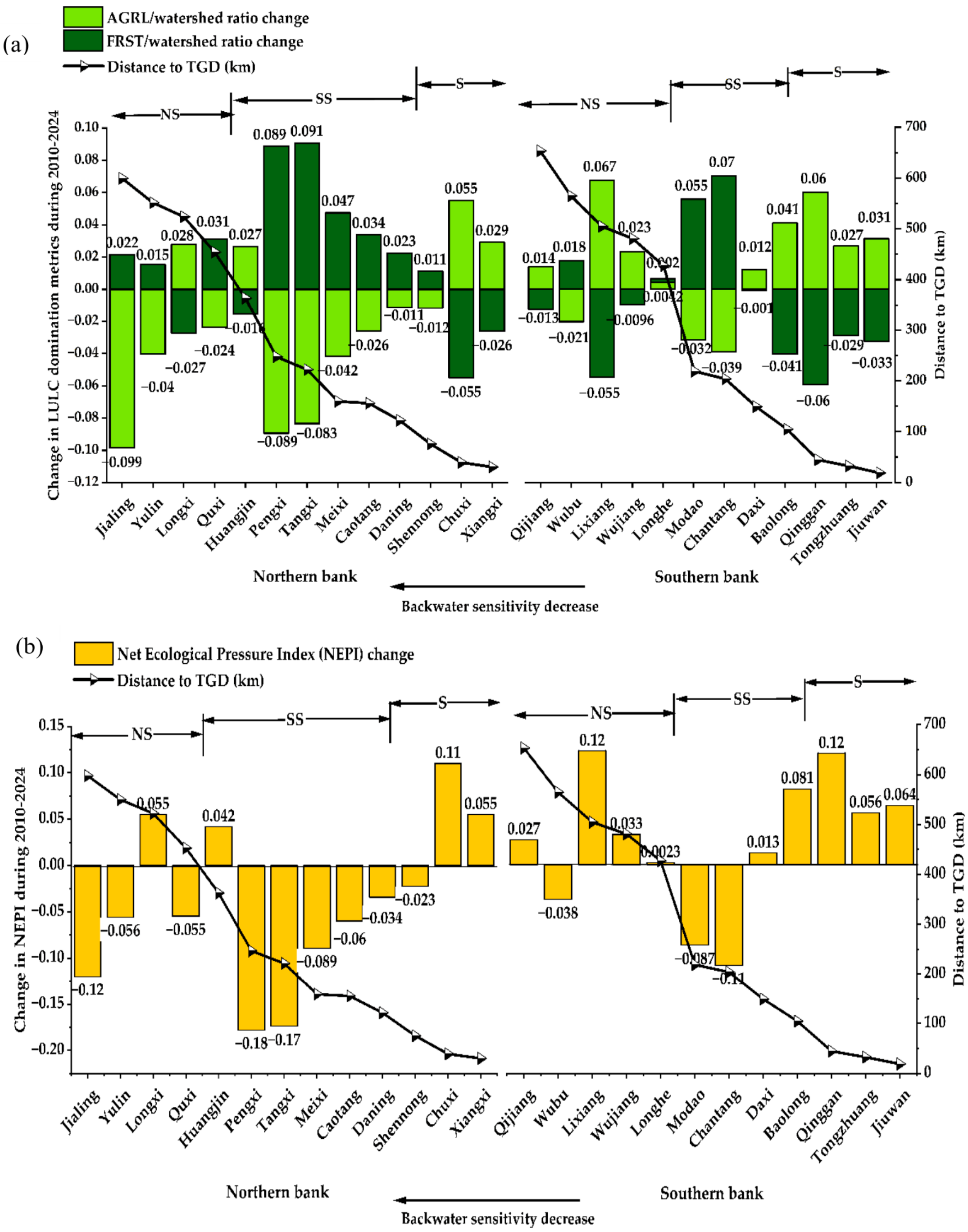

Figure 6. Temporal change for LULC domination metrics (a) , and NET Ecological Pressure Index (b) of the northern and southern bank 1st-order tributaries at watershed scale from 2010 to 2024 across TGR backwater sensitivity zones regarding distance to TGD S refers to' sensitive zone', SS refers to' sub- sensitive zone', NS refers to' non-sensitive zone' according to Xu et al. [19].

Preprints.org (www.preprints.org) | NOT PEER-REVIEWED | Posted: 29 April 2026 doi:10.20944/preprints202604.2015.v1

3.2. Identifying Distinct Spatio-Temporal Ecological Behavior of TGRR Banks Within Backwater Sensitivity Zones

3.2.1. Contrasting Spatial Ecological Behavior of TGRR Banks Within Backwater Sensitivity Zones

Although both northern and southern-bank tributaries revealed similar spatial gradient for LULC domination metrics and NEPI $_{ws}$ at watershed scale across backwater sensitivity zones aligning with distance gradient to the TGD (Figures 3 and 4), the spatial dynamics of these parameters in both banks differed markedly within each zone (Figure 7). Within the non-sensitive and sub-sensitive zones, the northern bank showed greater agricultural domination than the southern bank in 2010 and 2024.

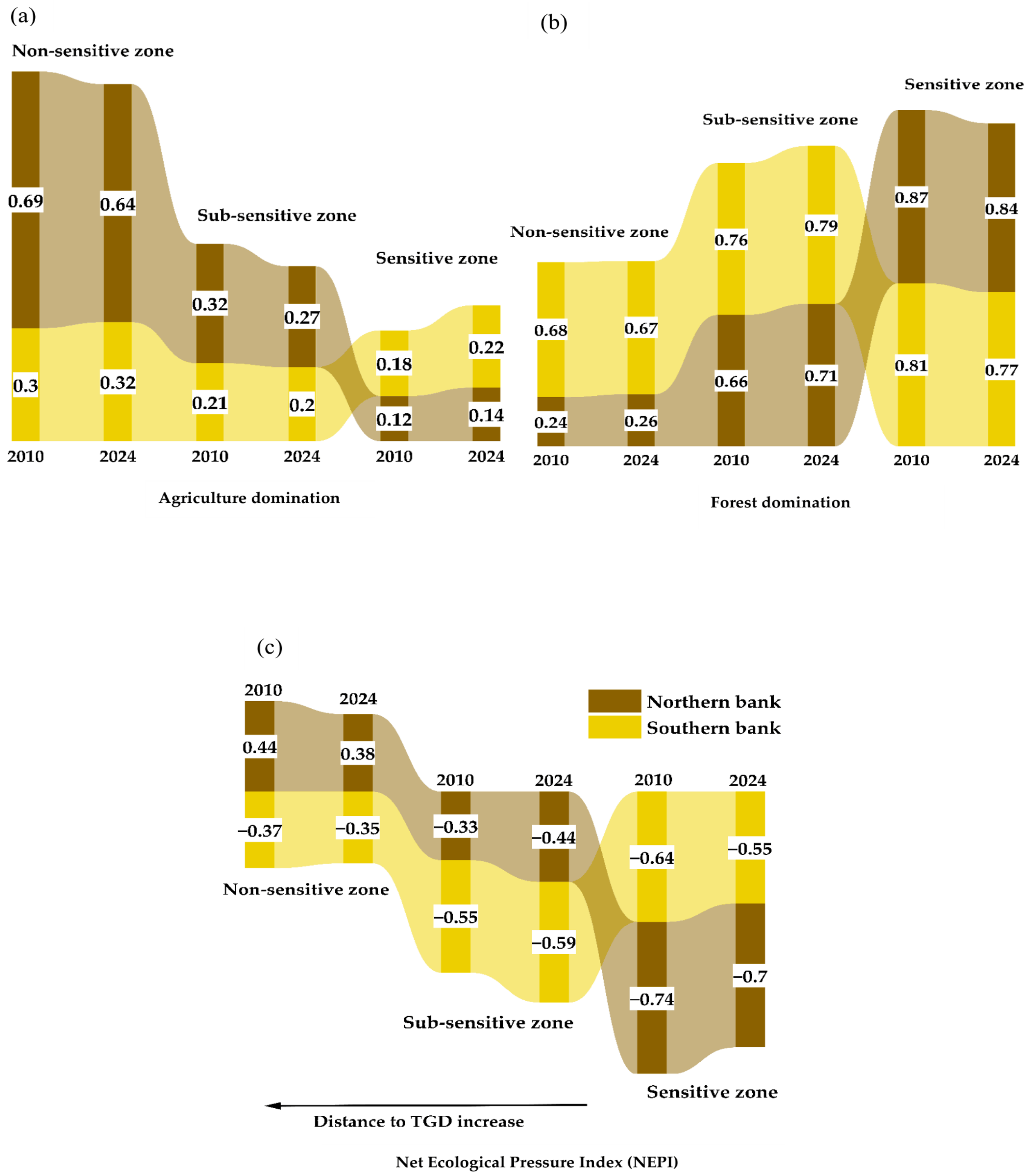

Figure 7. Transfer pathways of agriculture domination (a), forest domination (b) and Net Ecological Pressure Index (NEPI $_{bank}$) (c) for the northern and southern banks within TGR backwater sensitivity zones from 2010 to 2024.

In contrast, within the sensitive zone, agriculture was more dominant on the southern bank (Figure 7a). An opposite pattern was observed for forest domination (Figure 7b). The southern bank showed higher forest domination within the non-sensitive and sub-sensitive zones, whereas the northern bank exhibited greater forest domination within the sensitive zone. Subsequently, in 2010 and 2024, the northern and southern banks exhibited negative NEPI $_{bank}$ values across the TGR backwater sensitivity zones in 2010 and 2024, reflecting the domination of forest landcover relative to agricultural land over landscape (Figures 7). The only exception occurred on the northern bank within the non-sensitive zone, where NEPI $_{bank}$ values were positive (Figure 7c), indicating that agricultural domination exceeded forest domination over landscape (Figures 7a and 7b). In accordance with the contrasting LULC domination patterns, the northern bank exhibited higher NEPI $_{bank}$ values than the southern bank within the non-sensitive and sub-sensitive zones. Conversely, within the sensitive zone, this pattern was reversed, whereas the southern bank showed higher NEPI $_{bank}$ values than the northern bank (Figure 7c).

3.2.2. Contrasting Temporal Ecological Behavior of TGRR Banks Within Backwater Sensitivity Zones

Within the sensitive zone, the two banks exhibited the same directions, but contrasting magnitudes of change in LULC domination metrics (Figure 8a). Both banks experienced an increase in agricultural domination accompanied by a decrease in forest domination, but with different magnitudes (Figure 8a).

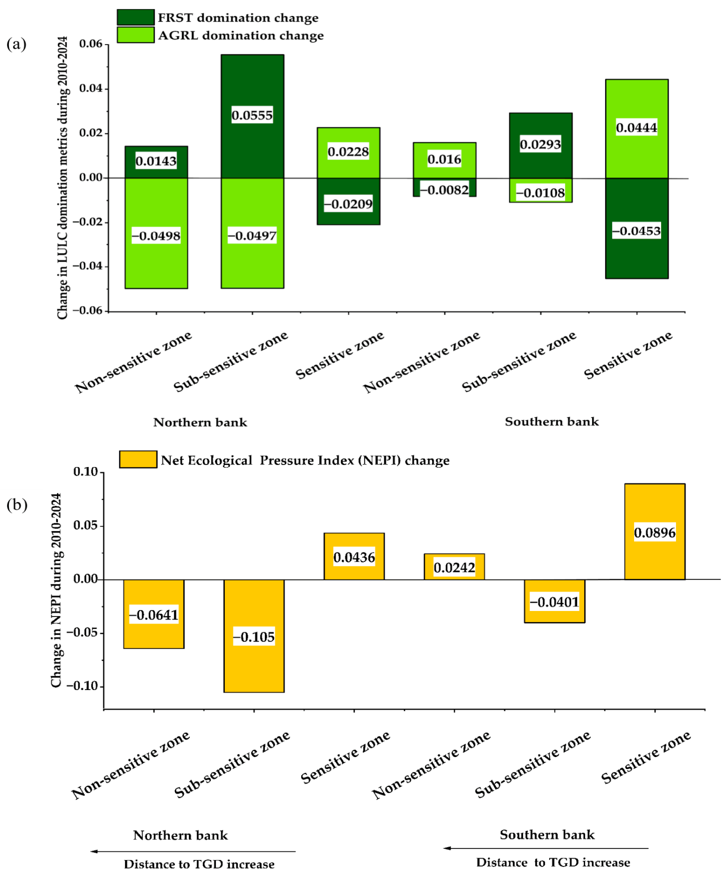

Figure 8. Temporal change of LULC domination metrics (a) and Net Ecological Pressure Index (b) for TGR backwater sensitivity zones within the northern and southern banks during 2010-2024.

From 2010 to 2024, the rise in agricultural domination with + 0.0444 on the southern bank was 1.94 times that of the northern bank with + 0.0228. Also, the decline in forest domination with – 0.0453 was 2.16 times greater that of the northern bank with -0.0209 (Figure 8a). Consistent with these temporal dynamics, the southern bank showed an increase with + 0.0896 in NEPI $_{bank}$ value which equaled 2.05 times that of the northern bank with + 0.0436 (Figure 8b).

Similarly, within the sub sensitive zone, the two banks exhibited the same directions, but differing magnitudes of change in LULC domination metrics (Figure 8a). However, compared with the sensitive zone, the two banks showed reversed directions and magnitudes of change (Figure 8a). Agricultural domination decreased, while forest domination increased for both banks with contrasting magnitudes (Figure 8a). From 2010 to 2024, the reduction in agricultural domination with – 0.0497 on the northern bank was 4.6 times that of the southern bank with – 0.0108, and the increase in forest domination with + 0.0555 was 1.89 times larger that of the southern bank with + 0.0293. Correspondingly, the northern bank showed a decline with - 0.105 in NEPI $_{bank}$ which equaled 2.61 times that of the southern bank with - 0.0401 (Figure 8b).

In contrast to the sensitive and sub-sensitive zones, the non-sensitive zone showed an entirely different behavior, as both banks exhibited opposing directions and differing magnitudes of change in LULC domination metrics (Figure 8a). The agricultural domination decreased with −0.0498 on the northern bank but increased with +0.016 on the southern bank. In contrast, forest domination increased with +0.0143 on the northern bank but decreased with −0.0082 on the southern bank (Figure 8a). Reflecting these divergent trends, NEPI $_{bank}$ also changed in opposing directions. The northern bank's NEPI $_{bank}$ decreased with −0.0641, while the southern bank's NEPI $_{bank}$ increased with +0.0242 (Figure 8b).

3.3. Unique Eco-Functional Zones (EFZs) Across the TGRR

3.3.1. Ranking the Eutrophication Vulnerability of EFZs Within TGR Sensitivity Zones

Within the sensitive zone, two EFZs were identified: EFZ1 and EFZ2 (Table 1 and Figure 9). Although both exhibited high Backwater-Induced Ecological Vulnerability (BIEV), EFZ2 consistently showed higher NEPI $_{bank}$ values than EFZ1 in 2010 and 2024 (Table 1), indicating greater NEPI $_{bank}$ spatial vulnerability. Both EFZs experienced an increase in NEPI $_{bank}$ from 2010 to 2024. However, EFZ2 revealed a larger magnitude of increase compared with EFZ1 (Table 1). Consequently, EFZ2 revealed higher NEPI $_{bank}$ temporal vulnerability compared with EFZ1 (Table 1). Within the sub-sensitive zone, two EFZs were also identified: EFZ3 and EFZ4 (Table 1 and Figure 9). Despite both being characterized by moderate Backwater-Induced Ecological Vulnerability (BIEV), EFZ3 exhibited higher NEPI $_{bank}$ value than EFZ4 in 2010 and 2024 (Table 1), indicating greater NEPI $_{bank}$ spatial vulnerability. Both EFZs experienced a decline in NEPI $_{bank}$ from 2010 to 2024. However, the magnitude of NEPI $_{bank}$ reduction was greater in EFZ3 compared with EFZ4 (Table 1). Consequently, EFZ4 revealed higher NEPI $_{bank}$ temporal vulnerability compared with EFZ3 (Table 1). Two EFZs were identified in the non-sensitive zone: EFZ5 and EFZ6 (Table 1 and Figure 9). Although both EFZs experiencing low Backwater-Induced Ecological Vulnerability (BIEV), EFZ5 showed higher NEPI $_{bank}$ values than EFZ6 (Table 1), indicating greater NEPI $_{bank}$ spatial vulnerability. However, their temporal trajectories diverged: EFZ5 exhibited a decrease in NEPI $_{bank}$ from 2010 to 2024, whereas EFZ6 showed an increase in NEPI $_{bank}$ over the same period (Table 1). Moreover, the magnitude of NEPI $_{bank}$ decline in EFZ5 was larger than the magnitude of NEPI $_{bank}$ increase in EFZ6. Consequently, EFZ6 revealed higher NEPI $_{bank}$ temporal vulnerability compared with EFZ5 (Table 1).

Table 1. Interpretation of Eco-Functional zoning codes within TGR sensitivity zones.

Backwater sensitivity zone	Eco-Functional zone	Zone code*	Spatial BIEV	Spatial LIEV	Drivers of temporal LIEV: NEPI bank change direction	Drivers of temporal LIEV: NEPI bank change magnitude	Temporal LIEV
Sensitive zone	EFZ1	H-L-L	High	Low	Increase	Low	Low
	EFZ2	H-H-H	High	High	Increase	High	High
Sub-sensitive zone	EFZ3	M-H-L	Moderate	High	Decrease	High	Low
	EFZ4	M-L-H	Moderate	Low	Decrease	Low	High
Non-sensitive zone	EFZ5	L-H-L	Low	High	Decrease	High	Low
	EFZ6	L-L-H	Low	Low	Increase	Low	High

* L refers to' Low', M refers to' Moderate', H refers to' High'.

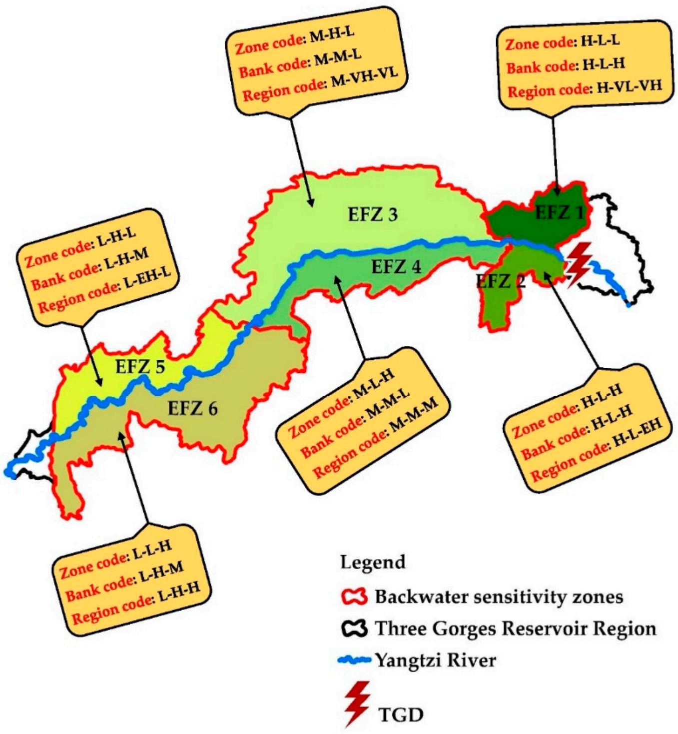

Figure 9. The distinctive Eco-Functional Zones (EFZs) of the Three Gorges Reservoir Region with coding labels for each EFZ within its sensitivity zone, within its bank and within the whole TGRR. VL refers to' Very low', L refers to' Low', M refers to' Moderate', H refers to' High', VH refers to' Very high', EH refers to' Extremely high'.

3.3.2. Ranking the Eutrophication Vulnerability of EFZs Along TGRR Banks

Along the TGRR northern bank, three Eco-Functional Zones (EFZs) were identified: EFZ1, EFZ3, and EFZ5 (Figure 9 and Table 2). Consistent with the gradient of backwater sensitivity, these EFZs exhibited contrasting levels of Backwater-Induced Ecological Vulnerability (BIEV), with vulnerability increasing closer to the Three Gorges Dam (Table 2). Accordingly, EFZ1 demonstrated the highest BIEV spatial vulnerability, followed by EFZ3, whereas EFZ5 exhibited the lowest BIEV spatial vulnerability along the northern bank (Table 2). Because NEPI $_{bank}$ showed an inverse spatial pattern relative to the backwater sensitivity gradient (Figure 7c), the three EFZs also revealed contrasting

Preprints.org (www.preprints.org) | NOT PEER-REVIEWED | Posted: 29 April 2026 doi:10.20944/preprints202604.2015.v1

NEPI $_{bank}$ spatial vulnerabilities, which increased with distance upstream from the dam. Consequently, EFZ5 exhibited the highest NEPI $_{bank}$ spatial vulnerability, followed by EFZ3, while EFZ1 exhibited the lowest NEPI $_{bank}$ spatial vulnerability along the northern bank (Table 2). Temporally, EFZ1 showed a slight increase in NEPI $_{bank}$ from 2010 to 2024, whereas EFZ3 and EFZ5 both experienced decreases in NEPI $_{bank}$ over the same period. However, the magnitude of decline was smaller in EFZ3 compared with EFZ5 (Table 1). As a result, EFZ1 exhibited the highest NEPI $_{bank}$ temporal vulnerability, followed by EFZ5, whereas EFZ3 exhibited the lowest NEPI $_{bank}$ temporal vulnerability along the northern bank (Table 2).

Along the TGRR southern bank, three Eco-Functional Zones (EFZs) were identified: EFZ2, EFZ4, and EFZ6 (Figure 9 and Table 2). Consistent with the backwater sensitivity gradient, these EFZs exhibited contrasting levels of Backwater-Induced Ecological Vulnerability (BIEV), with vulnerability increasing towards the Three Gorges Dam (Table 2). Accordingly, EFZ2 showed the highest BIEV spatial vulnerability, followed by EFZ4, whereas EFZ6 exhibited the lowest BIEV spatial vulnerability along the southern bank (Table 2).

Table 2. Interpretation of Eco-Functional zoning codes along TGRR banks.

Bank	Eco-Functional zone	Bank code*	Spatial BIEV	Spatial LIEV	Drivers of temporal LIEV		Temporal LIEV
					NEPI $_{bank}$ change direction	NEPI $_{bank}$ change magnitude	
Northern bank	EFZ1	H-L-H	High	Low	Increase	Low	High
	EFZ3	M-M-L	Moderate	Moderate	Decrease	High	Low
	EFZ5	L-H-M	Low	High	Decrease	Moderate	Moderate
Southern bank	EFZ2	H-L-H	High	Low	Increase	High	High
	EFZ4	M-M-L	Moderate	Moderate	Decrease	Moderate	Low
	EFZ6	L-H-M	Low	High	Increase	Low	Moderate

* L refers to' Low', M refers to' Moderate', H refers to' High'.

Because NEPI $_{bank}$ demonstrated an inverse spatial gradient relative to backwater sensitivity (Figure 7c), the three EFZs also revealed contrasting NEPI $_{bank}$ spatial vulnerabilities, which increased farther from the dam. Consequently, EFZ6 exhibited the highest NEPI $_{bank}$ spatial vulnerability, followed by EFZ4, whereas EFZ2 exhibited the lowest NEPI $_{bank}$ spatial vulnerability along the southern bank (Table 2). Temporally, EFZ4 experienced a moderate decrease in NEPI $_{bank}$ from 2010 to 2024, while both EFZ2 and EFZ6 showed increases in NEPI $_{bank}$ over the same period. However, the magnitude of increase was greater in EFZ2 than in EFZ6 (Table 2). As a result, EFZ2 exhibited the highest NEPI $_{bank}$ temporal vulnerability, followed by EFZ6, whereas EFZ4 exhibited the lowest NEPI $_{bank}$ temporal vulnerability along the southern bank (Table 2).

3.3.3. Ranking Eutrophication Vulnerability of EFZs Across the Whole TGRR

Across the TGRR, six Eco-Functional Zones (EFZs) were identified: EFZ1, EFZ2, EFZ3, EFZ4, EFZ5, and EFZ6. Consistent with the gradient of backwater sensitivity, EFZ1 and EFZ2 exhibited the highest Backwater-Induced Ecological Vulnerability (BIEV), followed by EFZ3 and EFZ4, whereas EFZ5 and EFZ6 showed the lowest BIEV across the TGRR (Figure 9 and Table 3). In response to the spatial NEPI $_{bank}$ gradients observed along both reservoir banks, and considering the contrasting NEPI $_{bank}$ values between the banks within each backwater sensitivity zone (Figure 7c), the EFZs across the TGRR were ranked as follows in terms of NEPI-based spatial vulnerability: EFZ5 > EFZ3 > EFZ6 > EFZ4 > EFZ2 > EFZ1.This ordering indicated that EFZ5 exhibited the highest NEPI $_{bank}$ spatial vulnerability, whereas EFZ1 exhibited the lowest NEPI $_{bank}$ spatial vulnerability across the entire TGRR (Figure 9 and Table 3). From 2010 to 2024, three EFZs exhibited an increase in NEPI $_{bank}$, i.e., EFZ1, EFZ2, and EFZ6, whereas the remaining three EFZs, i.e., EFZ3, EFZ4, and EFZ5, experienced a decline in NEPI $_{bank}$. Considering the relative magnitudes of increase and decrease among these EFZs, the overall temporal vulnerability ranking of NEPI $_{bank}$ across the TGRR followed the order: EFZ2 > EFZ1 > EFZ6 > EFZ4 > EFZ5 > EFZ3. This ranking indicated that EFZ2 exhibited the highest temporal vulnerability, while EFZ3 exhibited the lowest temporal vulnerability across the entire TGRR (Figure 9 and Table 3).

Table 3. Interpretation of Eco-Functional zoning codes across TGRR.

Region	Eco-Functional zone	TGRR code*	Spatial BIEV	Spatial LIEV	Drivers of temporal LIEV: NEPI $_{bank}$ change direction	Drivers of temporal LIEV: NEPI $_{bank}$ change magnitude	Temporal LIEV
TGRR	EFZ1	H-VL-VH	High	Very low	Increase	Moderate	Very high
	EFZ2	H-L-EH	High	Low	Increase	Very high	Extremely high
	EFZ3	M-VH-VL	Moderate	Very high	Decrease	Extremely high	Very low
	EFZ4	M-M-M	Moderate	Moderate	Decrease	Low	Moderate
	EFZ5	L-EH-L	Low	Extremely high	Decrease	High	Low
	EFZ6	L-H-H	Low	High	Increase	Very low	High

* VL refers to' Very low', L refers to' Low', M refers to' Moderate', H refers to' High', VH refers to' Very high', EH refers to' Extremely high'.

4. Discussion

4.1. Proof of Evidence and Interpretability of the Net Ecological Pressure Index (NEPI $_{ws}$)

The association between watershed-scale land-use/land-cover (LULC) composition and surface water quality is well established and supported by extensive empirical and process-based modeling research [30–33]. Empirical studies consistently demonstrated a negative correlation between agricultural land proportion and ecological water quality, while showed a positive correlation of forest cover with water quality indicators at the watershed scale [34,40].

Process-based watershed modeling studies certainly those utilizing the Soil and Water Assessment Tool (SWAT),further supported these empirical findings. SWAT-based simulations consistently show that agriculture-dominated watersheds exhibit higher surface runoff, sediment yield, and nutrient export to adjacent rivers compared to whereas forest-dominated watersheds [56-58]. Agriculture canopy is typically characterized by high curve number (CN2) values, low interception, and reduced surface roughness, conditions that promote surface runoff and erosion. When combined with intensive fertilizers application, croplands often act as major source of nutrient transport to rivers, i.e., nitrogen and phosphorus [59,60]. In contrast, forest vegetation is characterized by low curve number (CN2) values and high canopy interception which suppress surface runoff and sediment generation while enhancing nutrients retention and sediment trapping. Consequently, forest landcover function as effective sink for sediments and nutrients due to its strong ecological buffering capacity [23,24].

The Net Ecological Pressure Index (NEPI $_{ws}$) represents the difference between the upper limit and lower limit of ecological pressure exerted by landuse/landcover composition on river eutrophication. The upper limit of landscape ecological pressure can be reached in parts of watershed dominated by agricultural landuse which exert eutrophication promoting effect as the main source of surface water enrichment with nutrients and sediment. On the other hand, the lower limit of

 doi:10.20944/preprints202604.2015.v1

landscape ecological pressure can be reached in parts of watershed dominated by forest landcover which exert eutrophication buffering effect as the main sink and filter for nutrients and sediment generated from agriculture lands before reaching the adjacent surface water.

By subtracting forest domination ratio from agriculture domination ratio at watershed scale, the NEPI $_{ws}$ have the capability to identify the actual portion of agriculture ecological pressure that exceeded forest buffering capacity and contributed to surface water eutrophication. A positive NEPI $_{ws}$ value for a watershed indicates that agricultural pressure exceeds the ecological buffering capacity, thereby reflecting high ecological fragility. In contrast, negative NEPI $_{ws}$ value for a watershed indicates high capability of forest cover to neutralize agriculture negative impacts on water quality, reflecting stronger ecological resilience. Numerous studies have associated the ecological deterioration of tributary ecosystems to the proportions of agricultural land use and natural vegetation at the watershed scale [34-38]. Locke and Winter [34] demonstrated that approximately 80–90% natural vegetation cover is required at the watershed scale to maintain satisfactory water quality conditions in South African tributaries. Their threshold analysis further showed that when natural vegetation declines below 45%, pollution levels increase sharply, indicating a substantial loss of ecological buffering capacity. Similarly, a large scale study examining land use/land cover domination and eutrophication across 590 watersheds in eastern Canada found that in agriculture dominated watersheds, eutrophication intensified dramatically once the forest domination dropped below 47 % [35].

4.2. Understanding Spatial Interaction of Eutrophication Drivers Across TGRR

The differential eutrophication among TGRR 1st-order tributaries is governed by two key drivers the TGR operation regulations and watershed-scale LULC domination of 1st-order tributaries. Both drivers pose separate effects on eutrophication which is translated into a distinct ecological pressure exerted on TGRR tributaries, i.e., Backwater Ecological Pressure (BEP) and Net Landscape Ecological Pressure (NLEP) which can be estimated as function to distance from TGD and LULC domination spatial gradient, respectively. BEP as a tributary scale property, expressed the degree of the hydrologic regime alteration and the intrusion of nutrient enriched water from the main Yangtze River into tributaries through TGR backwater effect. In contrast, NLEP as a watershed-scale property, reflected the combined effect of agriculture and forest domination patterns on eutrophication. It reveals the net spatial interaction between the Agriculture Ecological Pressure that promotes sediment-nutrient transport cycle to river ecosystem and the Forest Ecological Buffering, which supports nutrient retention, sediment control and ecological resilience.

At watershed scale, the spatial dynamics of NEPI $_{ws}$ revealed inversed gradient compared to backwater sensitivity gradient along both TGRR banks (Figure 4). This implied that the Backwater Ecological Pressure (BEP) was the decisive factor governing susceptibility to eutrophication among the 1st-order tributaries within the sensitive zone. On contrary, NLEP was the decisive factor governing eutrophication evolution in the 1st-order tributaries within the non-sensitive zone. In contrast, both drivers exerted a shared influence on eutrophication evolution in 1st-order tributaries within the sub-sensitive zone. From another perspective, the positive NEPI $_{ws}$ values characterized the northern-bank watersheds within the non-sensitive zone compared to negative values for other watersheds across the entire TGRR (Figure 4), indicating landscape source-sink gradient [61,62]. Due to flat lands and relatively low elevations, the intensified agriculture production concentrated in this section of the northern bank act as a major source for reservoir water enrichment with nutrients which afterwards intrudes with tributaries estuary sections along TGRR during the impoundment stage [12,13,63,64]. On the other hand, due to the high elevations and steep slopes across the remaining parts of the TGRR, the possibility of agriculture expansion is dimensioned, keeping domination of forests over watershed landscape. This was reflected on landscape ecological function as nutrient sink [63,64].

Based on the cumulative NEPI $_{bank}$ at bank scale (Figure 7c), the spatial behavior of the northern bank across TGR backwater sensitivity zones, revealed higher contribution to the overall NLEP of the non-sensitive and sub-sensitive zones compared to the southern bank. On the other hand, the southern bank revealed higher contribution to the overall NLEP of the sensitive zone. This contrast spatial behavior characterizing each bank added a vertical dimension to the spatial variability of NLEP across TGRR. Several studies for the entire TGRR reported the spatial gradient of agriculture and forest domination patterns with respect to distance from TGD and confirmed its direct influence on the spatial distribution of agriculture non-point source pollution received by TGRR 1^{st}-order tributaries [40,65,66]. This supported the main claim of this study that contrasting LULC domination patterns between both TGRR banks enabled a distinct differentiated ecological function that can explain the differential eutrophic susceptibility of TGRR 1^{st}-order tributaries within the same backwater sensitivity zone.

4.3. Unveiling Temporal Trends of the Net Landscape Ecological Pressure (NLEP) Dynamics Across TGRR

The temporal dynamics of $NEPI_{bank}$ values indicated a distinct change in landscape ecological pressure for TGRR northern and southern banks across backwater sensitivity zones (Figure 8b).Mainly, previous studies for LULC transition in the TGRR [38,63,64], indicated that conversion of croplands into forest (afforestation) via ecological restoration projects, i.e., the Grain for Green Project was the key driver of the increase in forest area in expense of agriculture area. On contrary, the conversion of forest lands into croplands (deforestation) was the key driver of increasing agriculture area in expense of forest area. Accordingly, these continuous dynamics were reflected on the change in agriculture and forest domination patterns that shape landscape ecological pressure on river eutrophication across the region. Based on equations (1,6 and 9), the Net Landscape Ecological Pressure (NLEP) is conceptually defined as the net difference between Agricultural Ecological Pressure (AEP) which is function to agriculture domination and Forest Ecological Buffering (FEB) which function to forest domination at watershed and bank scales. Therefore, the changes in LULC domination patterns are directly reflected on the net expression of landscape ecological pressure and translated to whether improvement or deterioration in ecological resilience relying on change direction and magnitude.

In this context, the investigation of $NEPI_{bank}$ temporal dynamics across TGRR provided indicators for short-term and long-term monitoring of LULC transitions and ecological restoration projects. The general trend of $NEPI_{bank}$ temporal change from 2010 to 2024 across TGR backwater sensitivity zones tend to decrease on the northern bank while increase on the southern bank (Figure 8b). This trend reveal higher concentration for ecological restoration efforts on the northern bank compared to the southern bank. This was a response to the higher domination of agriculture activities on the northern bank compared to the southern bank (Figure 7a). Interestingly, along the northern bank, although characterized by lower agriculture domination (Figure 7a), the sub-sensitive zone received the higher concentration of ecological restoration efforts compared to the non-sensitive zone (Figure 8a).

Due to flat lands and relatively low elevations, agricultural production was intensified in the non-sensitive section of the northern bank. On the other hand, due to steeper and higher elevations characterizing the sub-sensitive zone the possibility for agriculture expansion was relatively diminished [63,64]. Due to the competing nature characterizing landuse functions, the balance between ecological and production spaces is a crucial constraint for implementation of ecological restoration projects [64]. For example, the implementation of the Grain for Green Project (GPP) in 2002 decreased the grain self-sufficiency index (GSSI) of the whole TGRR from 96 % in 2000 to 65 % in 2020 which exposed grain supply in the TGRR to a real risk [38].Therefor, the ecological policy planners do their best to leverage ecological benefits and decrease socio-economic severe impacts [67-70]. In this context, the eutrophication mitigation strategy in the non-sensitive section of the northern bank combined between afforestation and agricultural best management practices to achieve the balance between ecological benefits and sustainable agricultural production. While, in the sub-sensitive section, ecological restoration was implemented with relatively lower strict constraints [6,34].

 doi:10.20944/preprints202604.2015.v1

Despite this fact, it was more interesting that the non-sensitive section of the northern bank experienced almost the same magnitude of agriculture domination decrease as sub-sensitive section (Figure 8a).The previous studies of production- living-ecological spaces transition pathways in the TGRR, confirmed that a significant portion of agriculture domination decrease within the non-sensitive section on the northern bank was contributed to urban expansion in expense of croplands, demonstrating that afforestation was not the only driver of agriculture domination decrease in this area [63,64].

On the other hand, the increasing $NEPI_{bank}$ values characterizing both banks within the sensitive zone (Figure 8b), demonstrated the domination of deforestation due to croplands expansion in expense of forests in this area . These findings are consistent with Pan et al. [70], who reported similar trends in agricultural expansion and forest loss from 2010 to 2020 in Baodong, Zigui, and Xingshan counties within the sensitive zone. From ecological perspective, this fact raise long-term ecological pressure warning signs if the current trend continued. Within the sensitive zone, actually the backwater ecological pressure (BEP) demonstrating its higher limits closer to TGD and the continuous increase of agriculture expansion within this area is expected to amplify BEP and aggravate ecological pressure on aquatic ecosystems.

4.4. Interoperability, Comparability and Implications of NEPI

This study proposes the watershed-scale Net Ecological Pressure Index ($NEPI_{ws}$) as a physically interpretable indicator for monitoring landscape ecological pressure on river eutrophication. Because NEPI is constructed exclusively from land-use/land-cover (LULC) information derived from Earth observation platforms, it exhibits high interoperability across both spatial and temporal scales. Spatially, NEPI can be applied at sub-basin, watershed, or regional levels, enabling assessments that align with different hydrological units and administrative management needs. Temporally, NEPI can be derived at monthly, seasonal, or annual intervals, supporting short-term ecological diagnostics as well as long-term ecosystem monitoring and management.

A core strength of NEPI lies in its reliance on relative proportions of agricultural and forested land, rather than absolute land-use areas. This formulation substantially enhances comparability among watersheds of different sizes. Watersheds function as hydrologically independent units that contribute water, sediment, and nutrients to river systems [59], and numerous studies have demonstrated that pollutant export from watersheds is governed primarily by LULC composition rather than absolute land-use extent [72–75]. Consistent with these findings, the results of this study demonstrate that NEPIws_{ws}ws enables meaningful comparison between tributary watersheds and reservoir banks within the Three Gorges Reservoir Region, despite differences in total LULC areas. These outcomes confirm the spatial interoperability and transferability of the proposed indicator. The strong interoperability of NEPI is fundamentally enabled by its remote-sensing foundation. Satellite-derived LULC datasets provide spatially continuous coverage and standardized classification across large and topographically complex reservoir catchments, which cannot be achieved through field-based surveys alone. Field observations are often spatially fragmented, temporally inconsistent, and costly, particularly in regions characterized by rugged terrain and rapid land-use change [76,77]. In contrast, Earth observation data allow consistent assessment of catchment-scale landscape composition and pressure dynamics, ensuring temporal comparability across years, tributaries, and management stages. This temporal consistency is essential for detecting trends related to land-use transformation, agricultural expansion, and ecological restoration, which are difficult to capture through episodic field monitoring [76-79].

Beyond monitoring and comparison, NEPI has important implications for environmental management and decision support. Because it reflects early compositional shifts in landscape patterns, NEPI can be integrated into ecological early-warning systems to identify emerging ecological pressure before significant deterioration of aquatic ecosystem conditions occurs [80,81]. Moreover, NEPI has high potential for integration with watershed-scale physically based models, allowing the combination of remote-sensing-derived spatio-temporal coverage with process-based

 doi:10.20944/preprints202604.2015.v1

simulation of nutrient transport and export dynamics. Such integration can improve mechanistic understanding of spatio-temporal variability in non-point source pollution [82,83]. In addition, NEPI can serve as a constraint or objective indicator within multi-objective optimization frameworks for land-use allocation, supporting sustainable watershed planning while balancing ecological and socio-economic objectives [67,68]. It can also be coupled with ecosystem service assessment tools, such as the Integrated Valuation of Ecosystem Services and Tradeoffs (InVEST) model suite, to enhance ecological resilience without imposing severe adverse impacts on food security or regional livelihoods [69,70]. Collectively, these characteristics position NEPI as a scalable, transferable, and practically relevant remote-sensing-driven indicator for integrated water resources management in large reservoir systems.

4.5. Further Investigation, Methodological Limitations and Future Development

Although the components of the Net Ecological Pressure Index (NEPI) have been thoroughly validated and supported by a substantial body of literature, further investigation is required to elucidate the mechanistic pathways between the proposed NEPI and sediment–nutrient transport to surface waters via implying process-based modelling, certainly the Soil and Water Assessment Tool (SWAT) which have been widely applied to evaluate how land use/land cover (LULC) composition on surface water quality.

One of methodological limitations that dimension the temporal interoperability of NEPI is its formulation at an annual temporal scale, which restricts its ability to capture intra-annual and seasonal variations in landscape ecological sensitivity. Furthermore, the current NEPI formula characterizes agricultural land as a homogeneous land-use class, thereby representing only the overall ecological pressure of agriculture while neglecting crop-specific heterogeneity.

To tackle these limitations, the future development should concentrate on spatio-temporal downscaling of NEPI via integrating remote sensing–driven crop pattern mapping [47-50]. The rapidly expanding availability of high-temporal-resolution satellite observations, particularly from Sentinel-1 and Sentinel-2 missions, has revolutionized crop monitoring by enabling near-continuous tracking of vegetation phenology and management practices [51-54]. When combined with machine learning and transfer learning techniques, these datasets support highly accurate crop pattern classification across diverse agro-ecosystems, even in data-scarce regions [3,44]. Different crop types are characterized by distinct fertilization regimes, growth cycles, irrigation demands, and residue management practices, resulting in substantially heterogeneous nutrient export potentials even within aggregated agricultural landuse classes. Identifying the weighted dominance of specific crop types over agricultural landscapes therefore enables a more realistic representation of landscape ecological pressure.

By incorporating remote sensing–based crop type discrimination, NEPI can be downscaled from a coarse agricultural land-use level to a crop-pattern level, significantly increasing its spatial resolution and diagnostic capability. Such refinement allows NEPI to better capture intra-agricultural variability in nutrient source intensity. Also, it enables monitoring of seasonal land-use transitions and crop rotations, thereby enhancing the detection of time-varying ecological pressure signals. Remote sensing–based LULC change detection and phenological analysis can thus be used to uncover the dominant drivers of seasonal nutrient pressure, linking observed nutrient responses to underlying agricultural practices and landscape functioning processes.

5. Conclusions

Empowered by the spatio-temporal capabilities of remote sensing, this study developed the Net Ecological Pressure Index ($NEPI_{ws}$) to quantify watershed-scale landscape ecological pressure on river eutrophication. Derived from agricultural and forest dominance ratios based on land-use/land-cover data, $NEPI_{ws}$ ranges from −1 to 1, with positive values indicating agricultural domination and negative values indicating forest domination. The $NEPI_{ws}$ was implied to 25 1st-order tributaries in the Three Gorges Reservoir Region and revealed clear spatio-temporal heterogeneity in ecological pressure patterns. Spatially, NEPI $_{ws}$ increased along both banks as backwater sensitivity decreased farther from the Three Gorges Dam. The northern bank showed higher cumulative NEPI $_{bank}$ values than the southern bank within non-sensitive and sub-sensitive zones, whereas the opposite pattern occurred in the sensitive zone. Temporally, the southern bank showed a greater NEPI $_{bank}$ increase in the sensitive zone (+0.0896 vs. +0.0436), while the northern bank showed a stronger decline in the sub-sensitive zone (−0.105 vs. −0.0401). In the non-sensitive zone, NEPI $_{bank}$ decreased on the northern bank (−0.0641) but increased on the southern bank (+0.0242). Overall, NEPI effectively captured ecological pressure at both watershed and bank scales. Its standardized and transferable formulation enables comparative assessment, long-term monitoring, and spatial prioritization of eutrophication management in large reservoir systems, demonstrating the value of remote sensing data for integrated water resources management in mixed agricultural–forest landscapes.

Supplementary Materials: The following supporting information can be downloaded at: https://www.mdpi.com/article/doi/.

Author Contributions: Abdelrahman Hassan: Conceptualization, Data curation, Resources, Formal analysis, Methodology, Investigation, Visualization, Software, Writing – original draft, Writing – review & editing. Oluwafemi Adewole Adeyeye: Data curation, Resources, Formal analysis, Methodology, Investigation, Software, Writing – review & editing. Wei Huang: Resources, Visualization. Xiaojiao Luo: Resources, Visualization. Yemei Kong: Resources, Visualization. Bai Guoxin: Resources, Visualization. Zenghui Song: Resources, Visualization. Guanglang Yang: Resources, Visualization. Xuexing Yao: Resources, Visualization. Muhammad Waqas Yonas: Resources, Visualization. Amechi S. Nwankwegu: Investigation, Resources, Visualization. Yan Zhang: Resources. Shuai Wang: Writing – review & editing. Lei Zhang: Project administration, Supervision, Conceptualization, Resources, Formal analysis, Investigation, Writing – review & editing.

Funding: This research was funded by CHINA SCHOLARSHIP COUNCIL (CSC), grant number 2019GBJ003240 through awarding a full-time PhD scholarship for the first author of this paper.

Data Availability Statement: Data are contained within the article.

Acknowledgments: Thanks are forwarded to China Scholarship Council for providing a full-time PhD scholarship, received by the first author of this paper. Thanks also are extending to 216-lab group, College of Resources and Environment, Southwest University for supportive cooperation and help. During the preparation of this manuscript/study, the author(s) used [ChatGPT, Microsoft Copilot and Deep Seek] for the purposes of [improving readability and language of the manuscript]. The authors have reviewed and edited the output and take full responsibility for the content of this publication.

Conflicts of Interest: The authors declare no conflicts of interest.

Abbreviations

The following abbreviations are used in this manuscript:

TGRR	Three Gorges Reservoir Region
TGD	Three Gorges Dam
TGR	Three Gorges Reservoir
AEP	Agricultural Ecological Pressure
BEP	Backwater Ecological Pressure
FEB	Forests Ecological Buffering
NLEP	Net Landscape Ecological Pressure
NEPI	Net Ecological Pressure Index
BIEV	Backwater-Induced Ecological Vulnerability
LIEV	Landscape-Induced Ecological Vulnerability

 doi:10.20944/preprints202604.2015.v1

References

1. Steffen, W.; Broadgate, W.; Deutsch, L.; Gaffney, O.; Ludwig, C. The trajectory of the Anthropocene: The great acceleration. *Anthropocene Rev.* **2015**, *2*, 81–98. https://doi.org/10.1177/2053019614564785
2. Keys, P.W.; Galaz, V.; Dyer, M.; Matthews, N.; Folke, C.; Nyström, M.; Cornell, S.E. Anthropocene risk. *Nat. Sustain.* **2019**, *2*, 667–673.https://doi.org/10.1038/s41893-019-0327-x
3. Moghaddam, S.N.M.; Cao, H. *Artificial Intelligence Driven Geographies: Revolutionizing Urban Studies*; Springer: Singapore, 2024.https://doi.org/10.1007/978-981-15-0000-0
4. Kakade, A.; Salama, E.S.; Han, H.; Zheng, Y.; Kulshrestha, S.; Jalalah, M.; Harraz, F.A.; Alsareii, S.A.; Li, X. World eutrophic pollution of lakes and rivers: Biotreatment possibilities and future perspectives.*J.Environ.Chem. Eng.* **2021**, *9*, 101604.https://doi.org/10.1016/j.jece.2021.101604
5. Xia, R.; Zhang, Y.; Wang, G.; Zhang, Y.; Dou, M.; Hou, X.; Qiao, Y.; Wang, Q.; Yang, Z. Multi-factor identification and modeling analysis for managing large river algal blooms. *Environ. Pollut.* **2019**, *254*, 113056.https://doi.org/10.1016/j.envpol.2019.113056
6. Ministry of Environmental Protection of the People's Republic of China (MEP). *Bulletin on the Ecological and Environmental Monitoring Results of the Three Gorges Project (2018)*; MEP: Beijing, China, 2018.Available online: https://enlish.mee.gov.cn/Resources/Reports/(accessed on March 2026).
7. Qiu, W.; Zhong, Z.; Li, Z. Agricultural non-point source pollution in China: Evaluation, convergence characteristics, and spatial effects. *Chin. Geogr. Sci.* **2021**, *31*, 571–584.https://doi.org/10.1007/s11769-021-1200-1
8. Zou, L.; Liu, Y.; Wang, Y.; Hu, X. Assessment and analysis of agricultural non-point source pollution loads in China (1978–2017). *J. Environ. Manag.* **2020**, *263*, 110400.https://doi.org/10.1016/j.jenvman.2020.110400
9. Xu, Y.; Zhang, M.; Wang, L.; Kong, L.; Cai, Q. Changes in water types under regulated water-level operation in the Three Gorges Reservoir, China.*Quat. Int.* **2011**, *244*, 272–279.https://doi.org/10.1016/j.quaint.2011.01.019
10. Xiang, R.; Wang, L.; Li, H.; Tian, Z.; Zheng, B. Water quality variation in tributaries of the Three Gorges Reservoir from 2000 to 2015.*Water Res.* **2021**, *195*, 116993.https://doi.org/10.1016/j.watres.2021.116993
11. Yang, Z.; Wei, C.; Liu, D.; Lin, Q.; Huang, Y.; Wang, C.; Ji, D.; Ma, J.; Yang, H. Influence of hydraulic characteristics on algal blooms in the Three Gorges Reservoir, China.*Water Res.* **2022**, *211*, 118030. https://doi.org/10.1016/j.watres.2021.118030
12. Huang, Y.; Zhang, P.; Liu, D.; Yang, Z.; Ji, D. Nutrient spatial patterns of the upstream, mainstream, and tributaries of the Three Gorges Reservoir.*Environ. Monit. Assess.* **2014**, *186*, 6833–6847.https://doi.org/10.1007/s10661-014-3892-5
13. Yao, L.; Liu, L.; Su, Q.; Zhang, Y.; Wang, C. Fate and transport of nutrients and algal contaminants in Xiangxi Bay of the Three Gorges Reservoir.*Energy Environ. Eng.* **2019**, *6*, 17–33. https://doi.org/10.13189/eee.2019.060201
14. Zhang, S.; Liu, Y.; Wang, T. How land use change contributes to reducing soil erosion in the Jialing River Basin, China.*Agric. Water Manag.* **2014**, *133*, 65–73. https://doi.org/10.1016/j.agwat.2013.10.016
15. Liu, R.; Wang, Q.; Xu, F.; Men, C.; Guo, L. Impacts of manure application on SWAT model outputs in the Xiangxi River watershed.*J. Hydrol.* **2017**, *555*, 479–488.https://doi.org/10.1016/j.jhydrol.2017.10.044
16. Zhu, K.; Chen, L.; Li, L.; Wang, Y.; Yan, X.; Chen, J.; Feng, C.; Shen, Z.A new distributed model for predicting erosion-type pollution by integrating sediment connectivity and a watershed model. *Environ. Model. Softw.* **2023**, *162*, 105662.https://doi.org/10.1016/j.envsoft.2023.105662
17. Cheng, Y.; Mu, Z.; Wang, H.; Zhao, F.; Li, Y.; Lin, L. Water residence time in a typical tributary bay of the Three Gorges Reservoir.*Water* **2019**, *11*, 1585.https://doi.org/10.3390/w11081585
18. Ji, D.; Wells, S.A.; Yang, Z.; Liu, D.; Huang, Y.; Ma, J.; Berger, C.J. Impacts of water level rise on algal bloom prevention in a tributary of the Three Gorges Reservoir, China.*Ecol. Eng.* **2017**, *98*, 70–81.
19. Xu, Y.; Yu, S.; Liu, D.; Ma, J.; Chuo, M. Impact of Three Gorges Reservoir operations on hydraulic characteristics in the backwater region. *Water* **2024**, *16*, 2045.https://doi.org/10.3390/w16142045
20. Foden, W.B.; Young, B.E.; Akçakaya, H.R.; Garcia, R.A.; Hoffmann, A.A.; Stein, B.A.; Thomas, C.D.; Wheatley, C.J.; Bickford, D.; Carr, J.A.; et al. Climate change vulnerability assessment of species. *WIREs Clim. Change* **2019**, *10*, e551.https://doi.org/10.1002/wcc.551

21. Adger, W.N. Vulnerability. *Glob. Environ. Chang.* **2006**, *16*, 268–281.https://doi.org/10.1016/j.gloenvcha.2006.02.006
22. Turner, B.L., II; Kasperson, R.E.; Matson, P.A.; McCarthy, J.J.; Corell, R.W.; Christensen, L.; Eckley, N.; Kasperson, J.X.; Luers, A.; Martello, M.L.; et al. A framework for vulnerability analysis in sustainability science.*Proc. Natl. Acad. Sci. USA* **2003**, *100*, 8074–8079.https://doi.org/10.1073/pnas.1231335100
23. Cecílio, R.A.; Pimentel, S.M.; Zanetti, S.S. Modeling the influence of forest cover on streamflows. *Catena* **2019**, *178*, 49–58. https://doi.org/10.1016/j.catena.2019.02.008
24. Gong, Y.; Ji, X.; Hong, X.; Cheng, S. Correlation analysis of landscape structure and water quality. *Water* **2021**, *13*, 2075.https://doi.org/10.3390/w13152075
25. Li, J.; Yang, W.; Li, W.; Mu, L.; Jin, Z. Coupled hydrodynamic and water quality simulation of algal blooms. *Ecol. Eng.* **2018**, *119*, 97–108.
26. Zhao, Y.; Zheng, B.; Wang, L.; Qin, Y.; Li, H.; Cao, W. Mixing processes in a reservoir–river confluence. *Environ. Sci. Technol.* **2016**, *50*, 9907–9914.
27. Zhang, L.; Xia, Z.; Zhou, C.; Fu, L.; Yu, J.; Taylor, W.D.; Hamilton, P.B.; Van Cappellen, P.; Ji, D.; Liu, D.; et al. Surface density layers promote algal blooms. *Freshw. Sci.* **2020**, *39*, 722–734. https://doi.org/10.1086/710332
28. Li, X.; Zhang, J.; Wang, Y.; Chen, Z.; Liu, Y.A Functional Zoning Method in Rural Landscape Based on High Resolution Satellite Imagery. *Remote Sens.* **2023**, *15*, 4920.https://doi.org/10.3390/rs15204920.
29. Mo, W.; Zhao, Y.; Yang, N.; Xu, Ecological Function Zoning Based on Ecosystem Service Bundles and Trade-Offs: A Study of Dongjiang Lake Basin, China. *Environ. Sci. Pollut. Res.* **2023**, *30*, 40388–40404. https://doi.org/10.1007/s11356-022-24782-z
30. Zhou, Y.; He, J.; Feng, L.; Wang, B.; Chen, Y.; Miao, L. Multiscale impacts of landscape metrics on water quality. *Front. Environ. Sci.* **2025**, *13*, 1544078.https://doi.org/10.3389/fenvs.2025.1544078
31. Gay, E.T.; Martin, K.L.; Caldwell, P.V. Projected land use change and water quality degradation. *PLOS Water* **2025**, *4*, e0000313.https://doi.org/10.1371/journal.pwat.0000313
32. Giri, S.; Qiu, Z. Land use and water quality relationships: A review.*J. Environ. Manag.* **2016**, *173*, 41–48. https://doi.org/10.1016/j.jenvman.2016.02.029
33. Yao, S.; Chen, C.; He, M.; Cui, Z.; Mo, K.; Pang, R.; Chen, Q. Land use as an indicator for water quality prediction. *Ecol. Indic.* **2023**, *146*, 109768.https://doi.org/10.1016/j.ecolind.2022.109768
34. Locke, K.A.; Winter, K. Vegetation thresholds for water quality protection.*Sci. Total Environ.* **2024**, *945*, 173924.https://doi.org/10.1016/j.scitotenv.2024.173924
35. Clément, F.; Ruiz, J.; Rodríguez, M.A.; Blais, D.; Campeau, S. Landscape diversity and forest edge density regulate stream water quality.*Ecol. Indic.* **2017**, *72*, 627–639.https://doi.org/10.1016/j.ecolind.2016.09.001
36. Morse, J.; Welch, J.N.; Weinberg, A.; Szabo, P. *Forest Cover and Water Quality—Implications for Land Conservation*; Open Space Institute: New York, NY, USA, 2018.
37. Zhong, X.; Xu, Q.; Yi, J.; Jin, L. Threshold relationship between landscape pattern and water quality. *Environ. Sci. Pollut. Res.* **2022**, *29*, 44103–44118.https://doi.org/10.1007/s11356-022-18970-0
38. Chen, X.; Luo, Z.; Wang, Z.; Zhang, W.; Wang, T.; Su, X.; Zeng, C.; Li, Z. Trade-offs between grain supply and soil conservation. *Sci. Total Environ.* **2024**, *945*, 173786.https://doi.org/10.1016/j.scitotenv.2024.173786
39. Huang, C.; Zhao, D.; Fan, X.; Liu, C.; Zhao, G. Landscape dynamics and non-point source pollution control. *Environ. Impact Assess. Rev.* **2022**, *92*, 106696.https://doi.org/10.1016/j.eiar.2021.106696
40. Ye, L.; Chen, K.; Cheng, J.; Tan, L.; Zhang, M.; Zhang, X.; Cai, Q. Ecological water quality and land cover relationships. *Front. Environ. Sci.* **2023**,*11*, 1196089.https://doi.org/10.3389/fenvs.2023.1196089
41. Allan, J.D. Landscapes and riverscapes. *Annu. Rev. Ecol. Evol. Syst.* **2004**, *35*, 257–284. https://doi.org/10.1146/annurev.ecolsys.35.120202.110122
42. Caldwell, P.V.; Martin, K.L.; Vose, J.M.; Baker, J.S.; Warziniack, T.W.; Costanza, J.K.; Frey, G.E.; Nehra, A.; Mihiar, C.M. Forested watersheds provide the highest water quality. *Sci. Total Environ.* **2023**, *882*, 163550.https://doi.org/10.1016/j.scitotenv.2023.163550
43. Gu, Z.; Zeng, M. The use of artificial intelligence and satellite remote sensing in land cover change detection: Review and perspectives. *Sustainability* **2024**, *16*, 274.https://doi.org/10.3390/su16010274

44. Ma, Y.; Chen, S.; Ermon, S.; Lobell, D.B. Transfer learning in environmental remote sensing. *Remote Sens. Environ.* **2024**, *301*, 113924.https://doi.org/10.1016/j.rse.2023.113924
45. Oli, D.; Gyawali, B.R.; Upadhaya, S.; Gebremedhin, M.; Zourarakis, D.; Pokharel, B. Assessment of long-term ecological impact in the lower Levisa Watershed using remote sensing.*Ecol. Inform.* **2025**, *92*, 103530. https://doi.org/10.1016/j.ecoinf.2025.103530
46. Yang, Y.; Huang, X. The 30 m annual land-cover dataset and its dynamics in China from 1985 to 2024.*Earth Syst. Sci. Data* **2025**, *13*, 3907–3925.https://doi.org/10.5281/zenodo.15853565
47. Di, Y.; Dong, J.; You, N.; Li, Z.; Moreno-Martínez, Á.; Izquierdo-Verdiguier, E.; Sun, J.; Fu, P.30 m annual crop-type maps in Northeast China from 2001 to 2022. *Sci. Data* **2026**, *13*, 197.https://www.nature.com/articles/s41597-025-06516-1
48. Jiang, Y.; Lu, Z.; Li, S.; Lei, Y.; Chu, Q.; Yin, X.; Chen, F. Large-scale and high-resolution crop mapping in China using Sentinel-2 satellite imagery. *Agriculture* **2020**, *10*, 433.https://doi.org/10.3390/agriculture10100433
49. Dai, K.; Cheng, C.; Li, B.; Xie, Y.; Gomez, J.A.; Wang, Z.; Wu, X. Mapping the harvest area of a comprehensive set of crop types in China from 1990 to 2020.*Sci. Data* **2025**, *12*, 1371.https://doi.org/10.1038/s41597-025-05723-0
50. Li, X.; Yu, L. Mapping complex cropping patterns in China (2018–2021) at 10 m resolution. *Earth Syst. Sci. Data Discuss.* **2025**.https://doi.org/10.5194/essd-2025-679
51. Liu, M.; He, W.; Zhang, H.CN_Wheat10: A 10 m resolution dataset of spring and winter wheat distribution in China (2018–2024). *Earth Syst. Sci. Data* **2026**, *18*, 465–491.https://doi.org/10.5194/essd-18-465-2026
52. Chen, Y.; Xu, Z.; Xu, H.; Xu, Z.; Wang, D.; Yan, X. Mapping crop types and cropping patterns using multi-source satellite datasets in subtropical mountainous regions of China.*Remote Sens.* **2025**, *17*, 2282.https://doi.org/10.3390/rs17132282
53. Liu, L.; Kang, S.; Xiong, X.; Qin, Y.; Wang, J.; Liu, Z.; Xiao, X. Cropping intensity map of China at 10 m resolution. *Int. J. Appl. Earth Obs. Geoinf.* **2023**, *124*, 103504.https://doi.org/10.1016/j.jag.2023.103504
54. Li, L.; Friedl, M.A.; Xin, Q.; Gray, J.; Pan, Y.; Frolking, S. Mapping crop cycles in China using MODIS-EVI time series. *Remote Sens.* **2014**, *6*, 2473–2493.https://doi.org/10.3390/rs6032473
55. Dile, Y.; Srinivasan, R.; George, C. QGIS 3 Interface for SWAT (QSWAT3), Version 1.6; Texas A&M University: College Station, TX, USA, 2022.Available online: https://swat.tamu.edu/software/qswat/(accessed on March 2026).
56. Fang, S.; Deitch, M.J.; Gebremicael, T.G.; Angelini, C.; Ortals, C.J. Identifying critical source areas of non-point source pollution using SWAT modeling. *Water Res.* **2024**, *253*, 121286.https://doi.org/10.1016/j.watres.2024.121286
57. Zhang, J.; Wang, Y.; Zhao, L.; Sun, R.; Sun, J.; Wang, S.; Xu, S.; Yang, Z. Identification of key factors influencing monthly runoff using deep learning and process-based models. *Environ. Model. Softw.* **2026**, *199*, 106927.https://doi.org/10.1016/j.envsoft.2026.106927
58. Zhao, J.; Zhang, N.; Liu, Z.; Zhang, Q.; Shang, C. SWAT model applications: From hydrological processes to ecosystem services.*Sci. Total Environ.* **2024**, *931*, 172605.https://doi.org/10.1016/j.scitotenv.2024.172605
59. Neitsch, S.L.; Williams, J.R.; Arnold, J.G.; Kiniry, J.R. *Soil and Water Assessment Tool: Theoretical Documentation, Version 2009*; Texas Water Resources Institute: College Station, TX, USA, 2011.Available online: https://swat.tamu.edu/docs/(accessed on March 2026).
60. Nie, Y.; Huang, G.; Tong, S.; Chen, W.; Song, Y.; Wang, X.; Zhang, Q.; Jiang, P. Impacts of rice terraces and ponds on sediment and phosphorus loads. *J. Clean. Prod.* **2024**, *459*, 142560. https://doi.org/10.1016/j.jclepro.2024.142560
61. Yang, H.; Qi, Z.; Huang, W.; Li, B.; Cheng, G.; Cai, Y. Evaluating the impact of “source–sink” landscape composition and configuration changes on sediment yield in watersheds using a coupled multi-model framework. *J. Clean. Prod.* **2025**, *534*, 146998. https://doi.org/10.1016/j.jclepro.2025.146998

62. Wang, J.; Shao, J.; Wang, D.; Ni, J.; Xie, D. Identification of the "source" and "sink" patterns influencing non-point source pollution in the Three Gorges Reservoir Area. *J. Geogr. Sci.* **2016**, *26*, 1431–1448. https://doi.org/10.1007/s11442-016-1336-6
63. Zhang, H.; Tang, Q.; He, X.; Yang, Q. Land use function changes and trade-offs across topographic gradients. *J. Clean. Prod.* **2024**, *469*, 143233. https://doi.org/10.1016/j.jclepro.2024.143233
64. Zhu, X.; Gao, J. Characteristics of production–living–ecological space dynamics in the Three Gorges Reservoir Area. *Reg. Sustain.* **2024**, *5*, 100139. https://doi.org/10.1016/j.regsus.2024.100139
65. Pan, L.; Chen, Y.; Shi, D.; Gao, J.; Jiang, Y.; Liu, F. Spatiotemporal evolution of sloping farmland and erosion risk zones. *Resour. Environ. Sustain.* **2025**, *21*, 100255. https://doi.org/10.1016/j.resenv.2025.100255
66. Shen, Z.; Qiu, J.; Hong, Q.; Chen, L. Simulation of spatial and temporal distributions of non-point source pollution. *Sci. Total Environ.* **2014**, *493*, 138–146. https://doi.org/10.1016/j.scitotenv.2014.05.109
67. Escano Pulido, G.; Razavi, H.; Nejadhashemi, A.P.; Deb, K.; Linker, L. Large-scale multi-objective optimization for watershed planning. *IEEE Trans. Syst. Man Cybern. Syst.* **2024**. https://doi.org/10.1109/TSMC.2024.3361679
68. Dogouri, M.A.; Janatrostami, S.; Ashrafzadeh, A.; Pirmoradian, N. Stochastic multi-objective optimization for the water–food–energy nexus. *Sci. Rep.* **2026**, *16*, 1477. https://doi.org/10.1038/s41598-025-31197-6
69. Salata, S.; Garnero, G.; Barbieri, C.A.; Giaimo, C. Evaluation of nutrient retention using the InVEST model. *Land* **2017**, *6*, 48. https://doi.org/10.3390/land6030048
70. Caro, C.; Marques, J.C.; Cunha, P.P.; Teixeira, Z. Ecosystem services as a resilience descriptor using InVEST. *Ecol. Indic.* **2020**, *115*, 106426. https://doi.org/10.1016/j.ecolind.2020.106426
71. Pan, F.; Shu, N.; Wan, Q.; Huang, Q. Land use function transition and ecosystem service value effects. *Land* **2023**, *12*, 391. https://doi.org/10.3390/land12020391
72. Deasy, C.; Baxendale, S.A.; Heathwaite, A.L.; Ridall, G.; Hodgkinson, R.; Brazier, R.E. Advancing understanding of runoff and sediment transfer across scales. *Earth Surf. Process. Landf.* **2011**, *36*, 1749–1760. https://doi.org/10.1002/esp.2196
73. Deelstra, J.; Kværnø, S.H.; Granlund, K.; Sileika, A.S.; Gaigalis, K.; Kyllmar, K.; Vagstad, N. Runoff and nutrient losses during winter periods. *J. Environ. Monit.* **2009**, *11*, 602–609. https://doi.org/10.1039/b818998f
74. Kreiling, R.M.; Givens, C.E.; Baker, A.C.; Kiesling, R.L.; Dantoin, E.D.; Perner, P.M.; Sterner, S.P.; Gierke, K.J.; Reneau, P. Tributary cyanobacterial and nutrient transport effects on bloom initiation. *J. Great Lakes Res.* **2024**, *50*, 102409.
75. Zhang, Y.; Wu, M.; Yang, F.; Yao, Q. Effects of natural flood and sediment regulation on nutrient transport. *Appl. Geochem.* **2023**, *159*, 105853. https://doi.org/10.1016/j.apgeochem.2023.105853
76. Mashala, M.J.; Dube, T.; Mudereri, B.T.; Ayisi, K.K.; Ramudzuli, M.R. A systematic review on advancements in remote sensing for assessing and monitoring land use and land cover change impacts on surface water resources in semi-arid tropical environments. Remote Sens. 2023, 15, 3926.https://doi.org/10.3390/rs15163926
77. Netzer, M.S.; Sidman, G.; Pearson, T.R.H.; Walker, S.M.; Srinivasan, R. Combining global remote sensing products with hydrological modeling to measure the impact of tropical forest loss on water-based ecosystem services. Forests 2019, 10, 413.https://doi.org/10.3390/f10050413
78. Cheng, C.; Zhang, F.; Shi, J.; Kung, H.-T.What is the relationship between land use and surface water quality? A review and prospects from a remote sensing perspective. Environ. Sci. Pollut. Res. 2022, 29, 56887–56907.https://doi.org/10.1007/s11356-022-21348-x
79. Shohadie, S.F.; Habibzadeh, N.; Ahmadzadeh, H.; Atazadeh, E. Integrated remote sensing approach to assess the impact of land cover change on eutrophication in a semi-arid dam reservoir. Int. J. Environ. Sci. Technol. 2026, 23, 222.https://doi.org/10.1007/s13762-026-07048-w
80. Romanelli, A.; Lima, M.L.; Ondarza, P.M.; Esquius, K.S.; Massone, H.E. DPSIR-based decision support for eutrophication prevention. *Environ. Manag.* **2021**, *68*, 393–410. https://doi.org/10.1007/s00267-021-01498-3
81. Bonsdorff, E. Eutrophication: Early warning signals and future responses. *Ambio* **2021**, *50*, 753–758. https://doi.org/10.1007/s13280-020-01432-7

 doi:10.20944/preprints202604.2015.v1

82. Qi, Z.; Cai, Y.; Ye, Y.; Yang, H.; Cai, S.; Tan, Q.; Zhang, S.; Yang, Z. Integrating landscape source–transport–sink mechanisms into GeoAI. *Water Res.* **2026**, *291*, 125263. https://doi.org/10.1016/j.watres.2025.125263
83. Wan, W.; Han, Y.; Wu, H.; Liu, F.; Liu, Z. Application of the source–sink landscape method in agricultural non-point source pollution. *Agric. Water Manag.* **2021**, *252*, 106910. https://doi.org/10.1016/j.agwat.2021.106910

Disclaimer/Publisher's Note: The statements, opinions and data contained in all publications are solely those of the individual author(s) and contributor(s) and not of MDPI and/or the editor(s). MDPI and/or the editor(s) disclaim responsibility for any injury to people or property resulting from any ideas, methods, instructions or products referred to in the content.